Rev. Adv. Mater. Sci. 27 (2011) 115-145

NONLINEAR OPTICAL PROPERTIES OF IMPLANTED METAL NANOPARTICLES IN VARIOUS TRANSPARENT MATRIXES: A REVIEW

A.L. Stepanov

Laser Zentrum Hannover, 30419 Hannover, Germany
Kazan Federal University, 420018 Kazan, Russian Federation
Kazan Physical-Technical Institute, Russian Academy of Sciences, 420029 Kazan, Russian Federation

Received: February 02, 2011

Abstract. Composite materials containing metal nanoparticles (MNPs) are now considered as a basis for designing new photonic media for optoelectronics and nonlinear optics. One of the promising methods for fabrication of MNPs is ion implantation. Review of recent results on nonlinear optical properties of cupper, silver and gold nanoparticles in various transparent dielectrics and semiconductors as glasses and crystals are presented. Composites prepared by the low energy ion implantation are characterized with the growth of MNPs in thin layer of irradiated substrate surface. Fabricated structures lead to specific optical nonlinear properties for femto-, pico- and nanosecond laser pulses in wide spectral area from UV to IR such as nonlinear refraction, saturable and two-photon absorption, optical limiting. Nonlinear properties of implanted composites in near IR are considered in details.

1. INTRODUCTION

The search for new nanostructured materials is one of the defining characteristics of modern science and technology [1-6]. Novel mechanical, electrical, magnetic, chemical, biological, and optical devices are often the result of the fabrication of new nanostructured materials. The specific interest of this review is recent advantages in optical science and technology, such as development of nonlinear optical random metal-dielectric and metal-semiconductor composites based on metal nanoparticles (MNP) synthesized by ion implantation. Simultaneously with the search for and development of novel technologies intended for nanoparticle synthesis, substantial practical attention has been devoted to designing techniques for controlling the MNP size. This is caused by the fact that the optical properties of MNPs, which are required for various applications, take place up to a certain MNP dimension. In this content, ion implantation nanotechnology allows one to fabricate materials with almost any MNP structures, types of metals and their allows [7-9]; this opens new avenues one in engineering nanomaterials with desired properties. Such composites possess fascinating electromagnetic properties, which differ greatly from those of ordinary bulk materials, and they are likely to become ever more important with a miniaturization of electronic and optoelectronic components.

Nonlinear optics plays a key role in the implementation and development of many photonics techniques for the optical signal processing of information at enhanced speed. The fabrication of novel useful nonlinear optical materials with ultrafast time response, high resistance to bulk and surface laser damage, low two-photon absorption and, of course, large optical nonlinearities is a critical for implemen-

Corresponding author: A.L. Stepanov, e-mail: aanstep@gmail.com

tation of those applications. In additional, nonlinear materials for optical switching should be manufactured by processes compatible with microelectronics technology. Nonlinear materials with such characteristics are interesting for waveguide applications. The earliest studies of optical analogs to electronic integrated circuits – or integrated optics – were based on the recognition that waveguide geometries allowed the most efficient interaction of light with materials. Optoelectronic devices could be converted to all-optical configurations, with a number of technological advantages, by developing waveguide media with intensity-dependent refractive indices. Nonlinear optical switches must provide conversion of laser signal for pulse duration as short as from nano- to femtoseconds. The nonlinear properties of MNP-containing materials stem from the dependence of their refractive index and nonlinear absorption on incident light intensity. Giant enhancement of nonlinear optical response in a random media with MNPs is often associated with optical excitation of surface plasmon resonances (SPR) that are collective electromagnetic modes and they are strongly dependent on the geometry structure of the composite medium [4]. Therefore, MNP-containing transparent dielectric and semiconductor materials can be effectively applied in novel integrated optoelectronic devices.

Although both classic and quantum-mechanical effects in the linear optical response of MNP composites have been studied for decades [4], the first experimental results on the nonlinear optical effects in MNPs in ruby-glass was obtained quite recently in 1985 by Ricard *et al.* [10]. Driven by the interest in creating nonlinear optical elements with MNPs for applications in all-optical switching and computing devices, variety of experimental and theoretical efforts have been directed at the preparation of composite materials. In practice, to reach the strong linear absorption of a composite in the SPR spectra region, attempts are made to increase the concentration (filling factor) of MNPs. Systems with a higher filling factor offer a higher nonlinear susceptibility, when all other parameters of composites being the same.

MNPs hold great technological promise because of the possibility of engineering their electronic and optical properties through material design. The metal of choice are usually gold, silver, or copper, as these metals show SPP modes in the visible or near-infrared spectral range [4]. The advantages of devices based on MNP materials can be understood from the spectacular successes of quantum well materi-

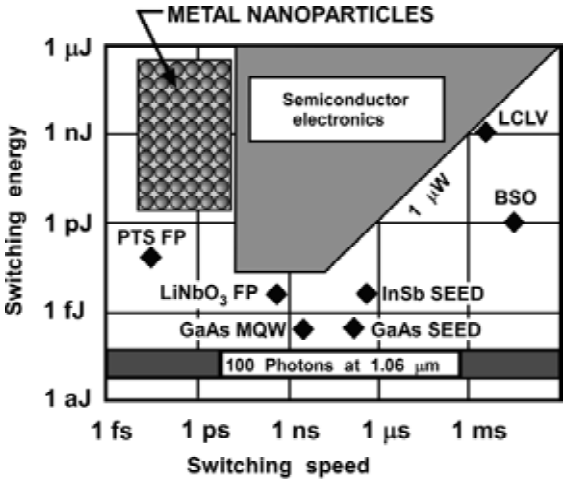

Fig. 1. Plot of various photonic materials showing their switching energies and switching speed. Adapted from [11,13].

als [11,12]. The capability of band gap engineering in these structures permits wavelength tuning, while their small size alters the electronic structure of these particles. This provides greater pumping efficiency and lower overall threshold for applications in optical limiting and switching. The potential advantages of MNP composites as photonic materials are substantial improvement in the signal switching speed. Up to 100 GHz repetition frequencies are expected in communication and computing systems of the 21th century [11]. Fig. 1 compares in graphical form the switching speed and switching energies of various electronic and optical materials and devices (adapted from [11,13]). Within the broad range of parameters covered by "conventional semiconductor microelectronics", current metal-oxide-semiconductor field-effect transistor devices made in silicon have low switching energies, but switching time in the nanosecond range. Photonic devices based on multiple quantum well (MQW) structures – SEED and GaAs MQW devices and Fabry-Perot (FP) cavities based on ferroelectric such as lithium niobate – have extremely low switching energies in comparison to MNPs, but relatively slow snitching speed [11,12].

Firstly Davenas *et al.* realized synthesis of MNPs in dielectrics by ion implantation in 1973 [14,15], when nanoparticles of various metals (sodium, calcium, etc.) in ionic crystals of LiF and MgO were created. Late in 1975, noble metal nanoparticles as Au and Ag were fabricated in silicate glasses by Arnold and Borders [16,17]. As shown in reviews

[7-9,18-23], now developments expanded from the singe metal implants to the use for formation of compounds, including metal allows and totally different composition precipitate inclusions. Implanted MNP were fabricated in various materials, as polymers, glass, artificial crystals, and minerals.

Number of publications on nonlinear optical properties of MNPs fabricated in transparent dielectric and semiconductor matrixes is increasing every year. There are some review articles observed partly this progress [11,18,19,24,25]. Unfortunately, some of this reviews are already quite old and do not reflect a modern knowledge of the field or restricted to numbers of selected publications. However, as followed from a comprehensive list of publications presented in Table 1 until 2011 [26-117], the geography of interest to nonlinear properties of ion-synthesized MNPs covers all world continents. The data in Table 1 includes information on all known types of metal ions and transparent matrices, ion implantation conditions for fabrication of MNPs and for measurements of their optical properties. Nonlinear optical characteristics of composites such as nonlinear refraction (n_2) and absorption (β) coefficients, real ($Re[\chi^{(3)}]$) and imaging parts ($Im[\chi^{(3)}]$) of third order nonlinear susceptibilities ($\chi^{(3)}$) and saturation intensities (I_{sat}) are presented as well. As shown in Table 1, near one hundred articles were already published. It should be mention, that ion implantation technique was first used for ion-synthesis of MNPs in dielectrics to create nonlinear optical materials in 1991 to form copper and gold nanoparticles in silica glass [42,100]. The present review focuses on advantages in nonlinear optical properties of MNPs fabricated generally by low-energy ion implantation and measured near IR spectral area.

2. OPTICS OF METAL NANOPARTICLE COMPOSITES

The nonlinear optical response of medium with MNPs can be described by expanding the *i*-th component of the polarization ***P*** induced by an applied optical field to third order in a power series in the applied in the applied electric field $\boldsymbol{E} = \boldsymbol{E}_0 e^{lex}$ [11,12]

$$P_i = \sum_j \chi_y^{(1)} E_j + \sum_{jk} \chi_{yk}^{(2)} E_j E_k + \sum_{jki} \chi_{yki}^{(3)} E_j E_k E_i + \ldots , \quad (1)$$

where the summation indices refer to Cartesian conditions in the material-dependent $\chi^{(q)}$ and to the polarization of the applied optical field.

The first-order susceptibility $\chi^{(1)}$ is related to the linear refractive index n_0 and the linear (Lambert-Beer's law) absorption coefficient through the following equation [13]

$$n_0 = \mathrm{Re}\left[1+\chi^{(1)}\right] \text{ and } \alpha_0 = \frac{\omega}{n_0 c}\mathrm{Im}\left[\chi^{(1)}\right], \quad (2)$$

where c – speed of the light, ω - the optical frequency. The value $\chi^{(3)}$ of a centrosymmetric composite has an analogous relationship to the nonlinear coefficients n_2 and β [45]

$$n_2 = \frac{12\pi}{n_0}\mathrm{Re}\left[1+\chi^{(1)}\right] \textit{ and } \beta = \frac{96\pi^2\omega}{n_0^2 c^2}\mathrm{Im}\left[\chi^{(1)}\right]. \quad (3)$$

The susceptibility $\chi^{(3)}$ is a fourth-rank tensor with eighty-one components; however, material symmetries often reduce the number of non-vanishing components substantially.

For a MNP with a dielectric constant $\varepsilon(\omega) = \varepsilon_1(\omega)+i\varepsilon_2(\omega)$ occupying a relative volume fraction (filling factor) $p << 1$ in a host of dielectric constant ε_h, the absorption can be presented as [45,118]

$$\alpha_0 = \frac{\omega}{n_0 c}\mathrm{Im}\left[\chi^{(1)}(\omega)\right] = 9p\frac{\omega\varepsilon_h^{3/2}}{c}\frac{\varepsilon_2}{\left(\varepsilon_1+2\varepsilon_h\right)^2+\varepsilon_2^2} = p\frac{\omega}{n_0 c}\left|f_1(\omega)\right|^2\varepsilon_2, \quad (4)$$

where the $f_1(\omega)$ is the mean-field enhancement factor. The linear absorption coefficient has a maximum at the SPR frequency [4] where $\varepsilon_1(\omega)+2\varepsilon_h(\omega)=0$.

The third-order nonlinear optical susceptibility of the dielectric medium with MNPs $\chi_{eff}^{(3)}$ can be derived by applying Maxwell's equations to the first order in the electromagnetic field to yield [3,119]

$$\chi_{eff}^{(3)} = p\left[\frac{3\varepsilon_h}{\varepsilon_1+2\varepsilon_h}\right]^2\left(\frac{3\varepsilon_h}{\varepsilon_1+2\varepsilon_h}\right)^2\chi_{met}^{(3)} = p\left|f_1\right|^2 f_1^2\chi_{met}^{(3)}, \quad (5)$$

where f_1 is the same local-field enhancement factor of the polarization describing the $\chi^{(1)}$ near or at the SPR. This equation shows that the nonlinearity of composites with MNPs comprises two factors: the nonlinearity due to the MNPs itself, and the enhancement contributed by the host matrix. Note that whereas the α_0 varies as $|f_1|^2$, the $\chi_{eff}^{(3)}$ varies as $|f_1|^2 f_1^2$. Hence, it is expected a significantly greater enhancement due dielectric nonlinearity in the $\chi_{eff}^{(3)}$.

Table 1. Types optically transparent dielectric and semiconductor matrixes with metal nanoparticles synthesized by ion implantation. Abbreviations: soda-lime silicate glass (SLSG), indium-tin oxide (ITO), degenerate four wave mixing (DFWM), pump-probe transient nonlinear spectroscopy (PPTNS), Z-scan, RZ-scan by reflection and vectorial self-diffraction (VSD).

Metal (Ion)	**Matrix**	**Synthesis conditions:** Energy (E), keV, Dose (D), ion/cm^2, Current density (J), μA/cm^2, Annealing temper. (T), °C and time	**Study nonlinear optical method**	**Laser parameters:** Wavelength (λ), nm, Pulse duration (τ), ps, Repetition rate (ν), Hz; Intensity (I_0), W/cm^2 Pulse energy (P), mJ	**Nonlinear parameters:** Refract. coef. (n_2), cm^2/W Absorption coef. (β), cm/W Satur. intensity (I_{sat}), W/cm^2 Re[$\chi^{(3)}$], *Im*[$\chi^{(3)}$], $\lvert\chi^{(3)}\rvert$, esu	**Authors**
Co	SiO_2	E = 50 $D = 4\times10^{16}$ J = 2	Z-scan	λ = 770 τ = 0.13 $\nu = 76\times10^9$ $I_0 = 11.4\times10^9$	$n_2 = 1.8\times10^{-9}$	Cattaruzza *et al.* 1998 [26]
Ni	SiO_2	E = 100 $D = 6\times10^{16}$	Z-scan	λ = 770 τ = 0.13 $\nu = 76\times10^9$ $I_0 = 9.8\times10^9$	$n_2 = 1.7\times10^{-10}$	Falconieri *et al.* 1998 [27] Cattaruzza *et al.* 2002 [28]
Cu	Al_2O_3	E = 40 $D = (0.5 - 1.0)\times10^{17}$ J = 2.5 - 12.5	RZ-scan	λ = 1064 τ = 55 ν = 2 $I_0 = 7.7\times10^9$	$n_2 = -(1.3 - 1.7)\times10^{-11}$ Re[$\chi^{(3)}$] = $-(1.0 - 1.4)\times10^{-9}$	Ganeev *et al.* 2005 [29]2006 [30] Ryasnyanskiy *et al.* 2005 [31]
Cu	Al_2O_3	E = 60	Z-scan	λ = 500 - 700 τ = 0.2 $\nu = 10^3$ $I_0 = 1.1\times10^7$	$\beta_{500\text{-}580} < 0$ $\beta_{580\text{-}700} > 0$	Plaksin *et al.* 2008 [32]
Cu	ITO	E = 40 $D = (0.5 - 7.5)\times10^{16}$ J = 4	Z-scan	λ = 532 $\tau = 7.0\times10^3$ ν = 10 $I_0 = (6.2 - 15.5)\times10^9$	$n_2 = (5.2 - 8.3)\times10^{-8}$ Re[$\chi^{(3)}$]=(5.4–7.4)×10^{-6} β=-(3.5–3.6)×10^{-3} Im[$\chi^{(3)}$]=-(1.2–1.3)×10^{-6} $\lvert\chi^{(3)}\rvert$=(5.5–7.5)×10^{-6}	Ryasnyanskiy *et al.* 2006 [33]

Cu	$LiNbO_3$	E = 60 D = (0.3 - 2.0)×10^{17} J = 10	PPTNS	λ = 574 τ = 0.2 ν = 10^3 P = 16	Bleaching absorption in 590-620 nm	Takeda *et al.* 2002 [34-36] Kishimoto *et al.* 2003 [37] Plaksin *et al.* 2005 [38]2006 [39]
Cu	$MgAl_2O_4$	E = 60 D = 3.0×10^{16} J = 10	DFWM	λ = 532	$\lvert\chi^{(3)}\rvert$ = (1.0 - 3.0)×10^{-8}	Kishimoto *et al.* 2000 [40]
Cu	MgO_2× Al_2O_4	E = 60 D = 3.0×10^{16} J = 1 - 100	PPTNS	λ = 574 τ = 0.2 ν = 10^3 P = 16	Bleaching absorption in 590-620 nm	Takeda *et al.* 2002 [34-36]2001 [41]
Cu	SiO_2	E = 160 D = 6.0×10^{16} J = 2 - 7.5	Z-scan	λ = 532 τ = 100 ν = 76×10^9 I_0 = 5.0×10^6	n_2 = 2.0×10^{-15}	Becker *et al.* 1991 [42] Haglund *et al.* 1992 [43]
Cu	SiO_2	E = 160	Z-scan	λ = 570 - 600 τ = 6 I_0 = 5.0×10^8	n_2 = (2.0 - 4.2)×10^{-10} Re[$\chi^{(3)}$] = 2.4×10^{-8} β = -(0.1 - 1.0)×10^{-6}	Haglund *et al.* 1993 [44]1994 [45] 1998 [46] Magruder *et al.* 1994 [47] Yang *et al.* 1994 [48]
Cu	SiO_2	E = 160 D = 1.2×10^{17} J = 0.7 - 7.5	DFWM	λ = 532 τ = 10 and 35	n_2 = 2.0×10^{-7} $\lvert\chi^{(3)}\rvert$ = (2.4 - 7.3)×10^{-8}	Haglund *et al.* 1994 [45]1998 [46] 1995 [42] Yang *et al.* 1994 [48]1996 [49]
Cu	SiO_2	E = 160 D = 1.2×10^{17} J = 2.5	Z-scan	λ = 532 τ = 100 ν = 76×10^9 I_0 = 1.0×10^7	n_2 = (2.0 - 4.2)×10^{-14} Re[$\chi^{(3)}$] = 2.4×10^{-8} β = -(3.0 - 8.0)×10^{-3}	Magruder *et al.* 1994 [47]

Cu	SiO_2	E = 90 D = 6×10^{16}	Z-scan	λ = 770 τ = 0.13 ν = 76×10^{9} I_0 = 9.8×10^{9}	n_2 = 5.0×10^{-11}	Falconieri *et al.* 1998 [27] Cattaruzza *et al.* 2002 [28]
Cu	SiO_2	E = 2.0×10^{3} D = $(1.0 - 4.0)\times10^{17}$ J = 2.0 T = 1000, 1 *h*	Z-scan	λ = 532 and 555 - 600 τ = 4.5 ν = 76×10^{9} I_0 = 8.8×10^{9}	n_2 =$(4.0 - 6.8)\times10^{-19}$ $\lvert\chi^{(3)}\rvert$ = $(0.3 - 4.7)\times10^{-7}$	Ilа *et al.* 1998 [50] Sarkisov *et al.* 1998 [51]
Cu	SiO_2	E = 60 D = 3.0×10^{16} J = 1 - 100	DFWM	λ = 532 and 561 τ = 7.0×10^{3} I_0 = $(0.1 - 1.0)\times10^{6}$	$\lvert\chi^{(3)}\rvert$ = $(0.2 - 2.2)\times10^{-8}$	Takeda *et al.* 1999 [52]2000 [53]
Cu	SiO_2	E = 50 D = 8.0×10^{16} J = 10	DFWM	λ = 585 τ = 13 ν = 400 I_0 = 1.0×10^{8}	$\lvert\chi^{(3)}\rvert$ = 1.0×10^{-7}	Olivares *et al.* 2001 [54]
Cu	SiO_2	E = 60 D = 3.0×10^{16} J = 1 - 30 T = 800, 1 *h*	PPTNS	λ = 574 τ = 0.2 ν = 10^{3} I_0 = 8.0×10^{11}	Bleaching absorption in 590-620 nm	Takeda *et al.* 2002[34-36, 55] 2001 [41]2004 [56,57]
Cu	SiO_2	E = 50 D = 8.0×10^{16} J = 10	Z-scan	λ = 354.7 τ = 55 ν = 2 I_0 = 4.1×10^{9}	n_2 = -0.6×10^{-7} $\mathrm{Re}[\chi^{(3)}]$ = -1.3×10^{-8} β = -6.7×10^{-6} $\mathrm{Im}[\chi^{(3)}]$ = -2.9×10^{-9} $\lvert\chi^{(3)}\rvert$ = 1.4×10^{-8}	Ganeev *et al.* 2003 [58]2004 [59]
Cu	SiO_2	E = 50 D = 8.0×10^{16} J = 10	Z-scan	λ = 532 τ = 55 ν = 2 I_0 = 5.4×10^{9}	β = -6.0×10^{-6} I_{sat} = 4.3×10^{8}	Ganeev *et al.* 2003 [60]2004 [61]
Cu	SiO_2	E = 50 D = 8.0×10^{16} J = 10	Z-scan	λ = 1064 τ = 35 ν = 2 I_0 = 1.0×10^{10}	n_2 = -1.4×10^{-7} $\mathrm{Re}[\chi^{(3)}]$ = -3.2×10^{-8} β = -9.0×10^{-6} $\mathrm{Im}[\chi^{(3)}]$ = 6.5×10^{-9} $\lvert\chi^{(3)}\rvert$ = 3.3×10^{-8}	Ganeev *et al.* 2003 [62, 63]2004 [64] Stepanov *et al.* 2003 [65]

Cu	SiO_2	E = 60 D = 1.0×10^{17} J = 10 T = 800, 1 h	Z-scan	λ = 540 - 610 τ = 0.2 ν = 1 I_0 = 8.0×10^{11}	$Re[\chi^{(3)}] = -3.1\times10^{-9}$ $Im[\chi^{(3)}] = 1.7\times10^{-9}$ $\lvert\chi^{(3)}\rvert = -(-1.6 - 3.1)\times10^{-8}$	Takeda *et al.* 2005 [66] Plaksin *et al.* 2008 [32]
Cu	SiO_2	E = 180 D = $(0.5 - 2.0)\times10^{17}$ J = 1.5 T = 500 - 900, 1 h	Z-scan	λ = 790 - 800 λ = 0.15 λ = 76×10^{9} I_0 = $(8.0 - 14.5)\times10^{9}$	$n_2 = -1.6\times10^{-10}$ $Re[\chi^{(3)}] = (0.9 - 1.4)\times10^{-7}$ $\beta = -(1.6 - 9.0)\times10^{-6}$ $Im[\chi^{(3)}] = (0.8 - 1.7)\times10^{-7}$ $\lvert\chi^{(3)}\rvert = (1.2 - 2.3)\times10^{-7}$	Ren *et al.* 2006 [67] Wang *et al.* 2006 [68, 69]
Cu	SiO_2	E = 100 - 200 D = 3.0×10^{16} T = 300 - 400, 1 h	Z-scan	λ = 533 τ = 7×10^{3} ν = 0.1 I_0 = 0.9×10^{9}	$n_2 = -3.7\times10^{-15}$ $Re[\chi^{(3)}] = 3.7\times10^{-12}$ $\beta = -(2.8 - 6.4)\times10^{-12}$ $Im[\chi^{(3)}] = 3.7\times10^{-14}$ $\lvert\chi^{(3)}\rvert = 3.7\times10^{-12}$ I_{sat} = $(2.9 - 5.0)\times10^{10}$	Ghosh *et al.* 2007 [70]2009 [71]
Cu	SiO_2	E = 2.0×10^{3} D = 4.0×10^{16} T = 900, 1 h	VSD	λ = 533 τ = 26 P = 16	$n_2 = -1.1\times10^{-12}$ $\beta = -2.0\times10^{-11}$ $\lvert\chi^{(3)}\rvert = 8.4\times10^{-11}$	Torres-Torres *et al.* 2008 [72]
Cu	SiO_2	E = 2.0×10^{3} D = 4.0×10^{16} T = 900, 1 h	VSD	λ = 533 τ = 7×10^{3} P = 16	$n_2 = -1.2\times10^{-11}$ $\beta = -2.0\times10^{-12}$ $\lvert\chi^{(3)}\rvert = 8.8\times10^{-10}$	Torres-Torres *et al.* 2008 [72]
Cu	SiO_2	E = 180 D = $(0.5 - 1.0)\times10^{17}$ J = 1.5	Z-scan	λ = 532 τ = 38 ν = 10 I_0 = 0.9×10^{9}	$n_2 = -(1.3 - 0.6)\times10^{-10}$ $\beta = -(458 - 151)\times10^{-9}$ $\lvert\chi^{(3)}\rvert = (2.1 - 0.8)\times10^{-7}$	Wang *et al.* 2009 [73] Wang *et al.* 2010 [74]
Cu	SiO_2	E = 180 D = $(0.5 - 1.0)\times10^{17}$ J = 1.5	Z-scan	λ = 1064 τ = 38 ν = 10 I_0 = 0.38×10^{9}	$n_2 = -(1.1 - 0.6)\times10^{-10}$ $\lvert\chi^{(3)}\rvert = (1.2 - 0.8)\times10^{-7}$	Wang *et al.* 2009 [73] Wang *et al.* 2010 [74,75]
Cu	SLSG	E = 50 D = 8.0×10^{16} J = 10	Z-scan	λ = 1064 τ = 35 ν = 2 I_0 = 3.0×10^{10}	$n_2 = 3.6\times10^{-8}$ $Re[\chi^{(3)}] = 0.8\times10^{-8}$ $\beta = -3.4\times10^{-6}$ $Im[\chi^{(3)}] = 2.5\times10^{-9}$ $\lvert\chi^{(3)}\rvert = 0.9\times10^{-8}$	Ganeev *et al.* 2003 [62,63]2004 [64] Stepanov *et al.* 2003 [65]

Cu	$SrTiO_3$	E = 60 $D = 3.0\times10^{16}$ J = 10	PPTNS	λ = 574 τ = 0.2 $\nu = 10^3$	Bleaching absorption in 605-690 nm and positive absorption in 516-506 nm	Takeda *et al.* 2002 [35,55]2004 [76]
Cu	$SrTiO_3$	E = 60 $D = 3.0\times10^{16}$ J = 10 T = 300, 1 h	Z-scan	λ = 540 - 610 τ = 0.2 ν = 1 $I_0 = 6.0\times10^{11}$	$Re[\chi^{(3)}] = -(0.1 - 2.0)\times10^{-9}$ $Im[\chi^{(3)}] = -(0.2 - 1.2)\times10^{-9}$ $\lvert\chi^{(3)}\rvert = (1.0 - 2.0)\times10^{-9}$	Takeda *et al.* 2006 [77]
Cu	$SrTiO_3$	$D = (0.1 - 1.0)\times10^{17}$	DFWMZ-scan	λ = 775 τ = 0.25 ν = 1	$n_2 = (1.8 - 6.2)\times10^{-12}$ $\lvert\chi^{(3)}\rvert = (1.6 - 5.33)\times10^{-10}$	Cetin *et al.* 2010 [77]
Cu	TiO_2	E = 60 $D = 3.0\times10^{16}$ J = 10	PPTNS	λ = 574 τ = 0.2 $\nu = 10^3$	Bleaching absorption in 585-760 nm	Takeda *et al.* 2002 [35]
Cu	ZnO	E = 160 $D = (0.1 - 1.0)\times10^{17}$ J = 20	Z-scan	λ = 532 τ = 55 ν = 2 $I_0 = 5.0\times10^8$	$\beta = -(0.4 - 2.1)\times10^{-3}$	Stepanov *et al.* 2004 [79] Ryasnyansky *et al.* 2005 [80]
Cu	ZnO	E = 160 $D = (0.1 - 1.0)\times10^{17}$ J = 20	Z-scan	λ = 532 $\tau = 7.5\times10^3$ ν = 10 $I_0 = 3.2\times10^7$	$\beta = -(0.7 - 5.5)\times10^{-3}$	Ryasnyansky *et al.* 2005 [80]
Ag	Al_2O_3	E = 30 $D = 3.8\times10^{17}$ J = 3 - 10	RZ-scan	λ = 1064 τ = 55 ν = 2 $I_0 = 4.3\times10^9$	$n_2 = (1.1 - 1.8)\times10^{-11}$ $Re[\chi^{(3)}] = (0.9 - 1.5)\times10^{-9}$	Ganeev *et al.* 2005 [29]2006 [30] Ryasnyanskiy *et al.* 2005 [81]
Ag	$LiNbO_3$	$E = 1.5\times10^3$ $D = 2.0\times10^{16}$ T = 500, 1 h	Z-scan	λ = 555 - 600 τ = 4.5 $\nu = 76\times10^6$ $I_0 = 8.8\times10^7$	$n_2 = (0.8 - 1.3)\times10^{-8}$	Sarkisov *et al.* 1998 [51]
Ag	$LiNbO_3$	$E = 1.5\times10^3$ $D = 2.0\times10^{16}$ T = 500, 1 h	Z-scan	λ = 532 τ = 40 - 70 ν = 10 $I_0 = 1.0\times10^{10}$	$n_2 = 5.0\times10^{-10}$	Williams *et al.* 1999 [82] Sarkisov *et al.* 2000 [83]

Ag	SiO_2	$E = 1.5\times10^3$ $D = 4.0\times10^{16}$ $J = 2$ T = 500, 1 h	Z-scan	$\lambda = 532$ $\tau = 4.5$ $\nu = 76\times10^6$	$\lvert\chi^{(3)}\rvert = 5.0\times10^{-7}$	Ila *et al.* 1998 [50]
Ag	SiO_2	$E = 60$ $D = 4.0\times10^{16}$ $J = 10$	Z-scan	λ=354.7 $\tau = 55$ $\nu = 2$ $I_0 = 1.3\times10^9$	$n_2 = -2.7\times10^{-7}$ $\mathrm{Re}[\chi^{(3)}] = -6.0\times10^{-8}$ $\beta = -1.4\times10^{-5}$ $\mathrm{Im}[\chi^{(3)}] = -6.1\times10^{-9}$ $\lvert\chi^{(3)}\rvert = 6.1\times10^{-8}$	Ganeev *et al.* 2003 [58]2004 [63]
Ag	SiO_2	$E = 60$ $D = 4.0\times10^{16}$ $J = 10$	Z-scan	$\lambda = 532$ $\tau = 55$ $\nu = 2$ $I_0 = (2.5 - 14)\times10^9$	$n_2 = -(6.2 - 0.7)\times10^{-10}$ $\mathrm{Re}[\chi^{(3)}] = -(3.5 - 0.4)\times10^{-8}$ $\beta = -(3.6 - 0.5)\times10^{-5}$ $\mathrm{Im}[\chi^{(3)}] = -(1.3 - 0.2)\times10^{-8}$	Ganeev *et al.* 2004 [84] Stepanov *et al.* 2010 [85]
Ag	SiO_2	$E = 60$ $D = 4.0\times10^{16}$ $J = 10$	Z-scan	$\lambda = 1064$ $\tau = 35$ $\nu = 2$ $I_0 = 1.0\times10^{10}$	$n_2 = 1.5\times10^{-8}$ $\mathrm{Re}[\chi^{(3)}] = 2.5\times10^{-9}$	Ganeev *et al.* 2003 [62]2004 [63]
Ag	SiO_2	$E = (1.7 - 2.4)\times10^3$ $D = (4.0 - 7.0)\times10^{16}$ $J = 0.3$ T = 500, 1 h	Z-scan	$\lambda = 532$ $\tau = 7.0\times10^3$ $P = 0.14$	Three-photon absorption	Joseph *et al.* 2007 [86]
Ag	SiO_2	$E = 2.0\times10^3$ $D = 7.0\times10^{16}$ T = 600, 1 h	Z-scan	$\lambda = 527$ $\tau = 0.233$ $\nu = \times10^3$	$\beta = -(2.6 - 1.8)\times10^{-6}$ $\mathrm{Im}[\chi^{(3)}] = 4.7\times10^{-10}$ $I_{sat} = (1.2 - 3.5)\times10^7$	Rangel-Rojo *et al.* 2009 [87]2010 [88]
Ag	SiO_2	$E = 200$ $D = 2.0\times10^{17}$ $J = 2.5$	Z-scan	$\lambda = 532$ $\tau = 38$ $\nu = 10$	$n_2 = -3.0\times10^{-11}$ $\mathrm{Re}[\chi^{(3)}] = 3.0\times10^{-8}$ $\beta = -7.0\times10^{-8}$ $\mathrm{Im}[\chi^{(3)}] = 2.6\times10^{-8}$ $\lvert\chi^{(3)}\rvert = 4.0\times10^{-8}$	Wang *et al.* 2009 [89]
Ag	SiO_2	$E = 200$ $D = 2.0\times10^{17}$ $J = 2.5$	Z-scan	$\lambda = 1064$ $\tau = 38$ $\nu = 10$	$n_2 = -1.7\times10^{-10}$ $\mathrm{Re}[\chi^{(3)}] = 1.8\times10^{-7}$ $\lvert\chi^{(3)}\rvert = 1.8\times10^{-7}$	Wang *et al.* 2009 [89]

Ag	SLSG	E = 60 D = 4.0×10^{16} J = 10	Z-scan	λ = 532 τ = 55 ν = 2 I_0 = (2.5 - 14)×10^9	n_2 = -(4.1 - 1.7)×10^{-10} Re[$\chi^{(3)}$] = -(2.4 - 1.4)×10^{-8} β = -(6.7 - 1.7)×10^{-5} Im[$\chi^{(3)}$] = -(0.6 - 2.4)×10^{-8}	Ganeev *et al.* 2004 [84]
Ag	SiO_2	E = 60 D = 4.0×10^{16} J = 10	Z-scan	λ = 1064 τ = 35 ν = 2 I_0 = 3.0×10^{10}	n_2 = 3.5×10^{-8} Re[$\chi^{(3)}$] = 5.7×10^{-9}	Ganeev *et al.* 2003 [63]2004 [64]
Sn	SiO_2	E = 400 D = 2.0×10^{17} J = 1	DFWM	λ = 460 - 540 τ = 5×10^3 I_0 = 3.0×10^{10}	|$\chi^{(3)}$|=3.0×10^{-6}	Takeda *et al.* 1993 [90]1994 [91]
Sn	SiO_2	E = 350 D = 8.0×10^{17} J = 2 T = 200, 0.5-1 h	Z-scan	λ = 460 - 540 τ = 4.5 ν = 76×10^6	|$\chi^{(3)}$|=1.5×10^{-6}	Ilа *et al.* 1998 [50]
Ta	SiO_2	E = 60 D = 3.0×10^{16} J = 0.3 T = 900, 1 h	PPTNS	λ = 574 τ = 0.2 ν = 10^3	Bleaching absorption in 502-605 nm	Takeda *et al.* 2003 [92]
Au	Al_2O_3	E = (2.75 - 3.0)×10^3 D = 2.2×10^{16} T = 1100, 1 h	DFWM	λ = 532 τ = 35 - 40 ν = 10 I_0 = 1.0×10^9	|$\chi^{(3)}$|=7.0×10^{-9}	White *et al.* 1993 [93]
Au	Al_2O_3	E = 160 D = (0.6 - 1.0)×10^{17} J = 10 T = 800 - 1100, 1 h	RZ-scan	λ = 1064 τ = 55 ν = 2 I_0 = (1.8 - 2.3)×10^9	n_2 = -(0.1 - 1.5)×10^{-10} Re[$\chi^{(3)}$] = -(0.8 - 1.2)×10^{-8}	Ganeev *et al.* 2005 [29]2006 [30] Stepanov *et al.* 2005 [94]2006 [95]
Au	Al_2O_3	E = 60 D = 2.0×10^{17} J = 10	PPTNS	λ = 568 τ = 0.2 ν = 10^3	Nonlinear dielectric functions	Takeda *et al.* 2006 [96]2007 [97]

Au	SiO_2	$E = 2.75\times10^3$ $D = (0.3 - 1.5)\times10^{17}$ T = 600 - 1100, 2.2 h	DFWMZ-scan	$\lambda = 532$ τ = 6 and 35 ν = 3.8 and 10 $I_0 = 4.5\times10^8$	$n_2 = (1.0 - 8.9)\times10^{-10}$ $\beta = (3.7 - 4.8)\times10^{-5}$ $\lvert\chi^{(3)}\rvert = (1.0 - 1.7)\times10^{-10}$	Haglund *et al.* 1994 [45] Yang *et al.* 1996 [49] Magruder *et al.* 1993 [98] White *et al.* 1994 [99]
Au	SiO_2	$E = 1.5\times10^3$ $D = 5.6\times10^{16}$ J = 0.7 T = 700 - 1200	DFWM	$\lambda = 532$ $\tau = 5\times10^3$ $I_0 = 1.0\times10^9$	$\lvert\chi^{(3)}\rvert = (0.12–5.0)\times10^{-8}$	Fukumi *et al.* 1991 [100]1994 [101]
Au	SiO_2	$E = 3.0\times10^3$ $D = 1.2\times10^{17}$ J = 2.0 T = 1200, 0.5-1 h	Z-scan	$\lambda = 532$ τ = 4.5 $\nu = 76\times10^6$	$\lvert\chi^{(3)}\rvert = 6.5\times10^{-7}$	Ila *et al.* 1998 [50]
Au	SiO_2	$E = 2.75\times10^3$ $D = 1.5\times10^{17}$ T = 400	DFWM	$\lambda = 532$ $\tau = 4\times10^3$ $I_0 = 1.9\times10^6$	$\lvert\chi^{(3)}\rvert = (0.3 - 1.3)\times10^{-7}$	Lepeshkin *et al.* 1999 [102] Safonov *et al.* 1999 [103]
Au	SiO_2	E = 60 $D = (1.0 - 2.0)\times10^{17}$ J = 10 - 17	PPTNS	λ = 554 and 568 τ = 0.2 $\nu = 10^3$ $I_0 = (0.7 - 0.9)\times10^9$	Nonlinear dielectric functions, positive absorption in 500-650 nm	Takeda *et al.* 2006 [96]2007 [104]
Au	SiO_2	$E = 2.0\times10^3$ $D = 2.8\times10^{16}$ T = 1100, 1 h	VSD	$\lambda = 532$ $\tau = 7\times10^3$ P = 0.14	$n_2 = -2.0\times10^{-8}$ $\mathrm{Re}[\chi^{(3)}] = 1.9\times10^{-9}$ $\beta = -5.0\times10^{-6}$ $\mathrm{Im}[\chi^{(3)}] = -1.6\times10^{-9}$ $\lvert\chi^{(3)}\rvert = 2.2\times10^{-9}$	Torrres-Torres *et al.* 2007 [105]
Au	SiO_2	$E = 1.5\times10^3$ $D = (0.3 - 1.0)\times10^{17}$ T = 400, 1 h	Z-scan	$\lambda = 532$ $\tau = 7\times10^3$ ν = 0.1 $I_0 = 1.2\times10^{10}$	$n_2 = -1.5\times10^{-11}$ $\mathrm{Re}[\chi^{(3)}] = 1.5\times10^{-8}$ $\beta = -(2.6 - 8.0)\times10^{-8}$ $\mathrm{Im}[\chi^{(3)}] = -1.5\times10^{-10}$ $\lvert\chi^{(3)}\rvert = 1.5\times10^{-8}$	Ghosh *et al.* 2008 [71]2009 [106]
Au	SiO_2	E = 250 - 300 $D = 1.0\times10^{17}$ J = 2.5	Z-scan	$\lambda = 532$ τ = 38 ν = 10 $I_0 = 0.9\times10^9$	$n_2 = -(1.2 - 1.4)\times10^{-10}$ $\mathrm{Re}[\chi^{(3)}] = -1.2\times10^{-7}$ $\beta = -(9.7 - 21.0)\times10^{-10}$ $\mathrm{Im}[\chi^{(3)}] = -3.6\times10^{-8}$ $\lvert\chi^{(3)}\rvert = (1.3 - 1.6)\times10^{-7}$	Wang *et al.* 2008 [107, 108]

Au	SiO_2	E = 250 - 300 $D = 1.0\times10^{17}$ J = 2.5	Z-scan	λ = 1064 τ = 38 ν = 10 $I_0 = 3.8\times10^{8}$	$n_2 = -0.4\times10^{-10}$ $Re[\chi^{(3)}] = -(4.3 - 1.2)\times10^{-8}$ $\lvert\chi^{(3)}\rvert = (0.1 - 4.3)\times10^{-8}$	Wang *et al.* 2008 [107, 108]
Cu-Ni	SiO_2	E = 90 and 100 $D = 6\times10^{16}$ and 6×10^{16}	Z-scan	λ = 770 τ = 0.13 $\nu = 76\times10^{9}$ $I_0 = 9.8\times10^{9}$	$\lvert\chi^{(3)}\rvert = 6.8\times10^{-10}$	Falconieri *et al.* 1998 [27] Cattaruzza *et al.* 2002 [28]
Cu-Ni	SiO_2	E = 90 and 100 $D = 6\times10^{16}$ and 6×10^{16}	Z-scan	λ = 532 τ = 6 ν = 0.5 - 1 $I_0 = 2.0\times10^{9}$	$n_2 = 1.5\times10^{-10}$ $\lvert\chi^{(3)}\rvert = 5.0\times10^{-12}$	Cattaruzza *et al.* 2002 [28] Battaglin *et al.* 2000 [109]
Cu-Ag	SiO_2	E = 160 and 305 $D = 1.2\times10^{16}$ J = 1.3 - 3	Z-scan	λ = 570 τ = 6 $\nu = 3.8\times10^{6}$ $I_0 = 4.0\times10^{8}$	$n_2 = (0.1 - 1.6)\times10^{-9}$ $\beta = -(1.4 - 3.8)\times10^{-5}$	Magruder *et al.* 1994 [110]
Cu-Ag	SiO_2	E = 30 and 43 $D = (1.0 - 2.0)\times10^{17}$	Z-scan	λ = 790 τ = 0.15 $\nu = 76\times10^{9}$ $I_0 = 8.8\times10^{9}$	$n_2 = -(3.8 - 4.3)\times10^{-12}$ $\beta = (1.0 - 2.2)\times10^{-6}$ $\lvert\chi^{(3)}\rvert = (0.8 - 1.5)\times10^{-8}$	Wang *et al.* 2007 [111]
Cu-Ag	SiO_2	E = 180 and 200 $D = (1.0 - 2.0)\times10^{17}$ J = 1.5 - 2.5	Z-scan	λ = 1064 τ = 38 ν = 10	$n_2 = (0.6 - 3.0)\times10^{-10}$ $\lvert\chi^{(3)}\rvert = (0.6 - 2.1)\times10^{-7}$	Wang *et al.* 2008 [112] 2010 [113,114]
Ag-Au	SiO_2	E = 130 and 190 $D = 9.0\times10^{16}$ J = 2 T = 800, 1 h	Z-scan	λ = 572 τ = 5 ν = 1 $I_0 = (1.6 - 5.0)\times10^{9}$	$n_2 = -1.6\times10^{-10}$ $\beta = 1.3\times10^{-5}$ $\lvert\chi^{(3)}\rvert = (0.9 - 1.7)\times10^{-8}$	Cattaruzza *et al.* 2003 [115]2005 [116]
Ti-Au	SiO_2	E = 320 and 1.1×10^{3} $D = (0.6 - 2.0)\times10^{16}$ T = 900, 2 h	Z-scan	λ = 532 τ = 6 $\nu = 3.8\times10^{6}$ $I_0 = 4.0\times10^{8}$	$n_2 = (0.6 - 1.2)\times10^{-9}$ $\beta = 5.3\times10^{-6}$	Magruder *et al.* 1995 [117]

3. NONLINEAR OPTICAL PROPERTIES OF ION-SYNTHESIZED NANOPARTICLES NEAR IR-AREA (1064 NM)

3.1. Nonlinear absorption and optical limiting of MNPs studied by Z-scan

In numerous studies, the nonlinear optical characteristics of the composite materials with MNPs fabricated by various methods were generally studied using lasers operating at frequencies that correspond to the spectral range of the SPR in particles [119] and Table 1. On other hand, one should take into account that, when used in practice as optical switches, optical limiters, and so on, these nonlinear materials should operate at the wavelengths of the most frequently used industry available lasers, such as Nd:YAG (λ = 1064 nm), Ti:Al_2O_3 (λ = 800 nm), and so on. Hence, in order to create new materials promising for practical use in laser systems and integral optics and to optimize their characteristics, one should study the nonlinear optical properties of these materials not only in the SPR spectral region, but also at the frequencies specific for industrial lasers. Materials characterized with nonlinear properties in near IR are now searching for applications in the field of telecommunication.

Here, recent results on nonlinear optical properties of copper and silver nanoparticles [62-65], synthesized by ion implantation in glass host matrices studied by the classical Z-method [120,121] at the wavelength of a picosecond mode-locked Nd:YAG laser (λ = 1064 nm) are presented. The used Z-scan setup is presented in Fig. 2. Laser pulse duration was 35 ps, pulse energy 1 mJ and 2-Hz pulse repetition rate. Our radiation had a spatial distribution close to Gaussian. Laser radiation was focused by a 25-cm focal length lens (1) onto the samples (2). The beam-waist diameter of the focused radiation was measured to be 90 μm using a CCD camera. The samples were transferred in steps of 2 nm along Z-axis when scanning focal region. The maximum laser intensity at the focal point was 3×10^{10} W/cm^2, whereas the intensities of optical breakdown were 6×10^{10} W/cm^2 and 8×10^{10} W/cm^2 for the glasses with copper and silver nanoparticles, respectively. The fluctuations of the laser energy from pulse to pulse did not exceed 10%. The energy of single laser pulses was measured by a calibrated photodiode (3). The samples were moved by a translation stage (7) along the Z-axis. A 1-mm aperture (A) with

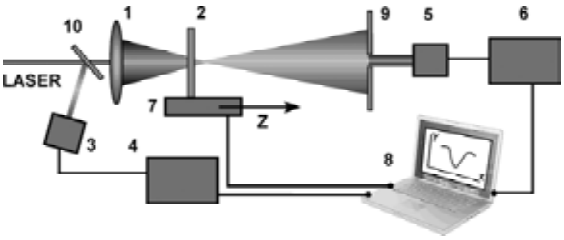

Fig. 2. Experimental Z-scan setup for nonlinear measurements.

1% transmittance was fixed at the distance of 100 cm from the focusing plane (closed-aperture scheme). A photodiode (5) was kept behind the aperture. The radiation energy registered by photodiode (5) was normalized relative to the radiation energy registered by photodiode (1) in order to avoid the influence of non-stability of laser parameters. The experimental data accepted as normalized transmittance $T(z)$. The closed-aperture scheme allowed the determination a value of n_2 and the open-aperture scheme was used for the measurements a value of β.

The samples with copper were prepared by Cu-ion implantation into amorphous SiO_2 and soda lime silicate glasses (SLSG) as described in details [65]. The energies of 50 keV and dose 8×10^{16} ion/cm^2 and at a beam current density of 10 μA/cm^2 were used. The penetration depth of the MNPs in the glasses for given energy of implantation was not exceed 80 nm. Optical transmittance spectra of implanted samples Cu:SiO_2 and Cu:SLSG are presented in Fig. 3. MNPs such as Cu in dielectric medium show optical absorption determined by SPR [4]. The spectra are maximized near 565 nm Cu:SiO_2 and 580 nm for Cu:SLSG that gives evidence for formation of the Cu nanoparticles in the glasses. Depending on the ion implantation conditions, the incorporation of accelerated ions into silicate glasses leads to the generation of radiation-induced defects, which can initiate reversible and irreversible transformations in the glass structure [6]. This can result in structural imperfections of different types, such as the generation of extended and point defects, local crystallization and amorphization, the formation of a new phase either from atoms involved the glass structure or from implanted ions, etc. In particular, the formation of MNPs in the glass brings about an increase in its volume and the generation of internal stresses within an implanted layer. The radiation-induced defects are responsible for an increase in the absorption in the range of the UV fun-

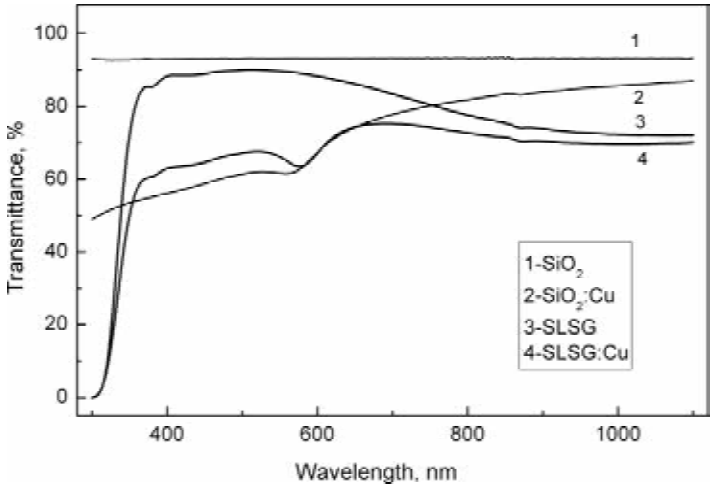

Fig. 3. Transmittance spectra of (1) SiO_2 and (2) SLSG before and after Cu-ion implantation with energy of 40 keV and dose of 8×10^{16} ion/cm^2 (3) Cu:SiO_2 and (4) Cu:SLSG [65].

damental absorption edge in the spectrum of the glass. In our case, this effect can be observed in the short-wavelength range of the optical transmittance spectra displayed in Fig. 3. It should be noted that, presented here nonlinear optical study were performed upon exposure of the samples to laser radiation at a wavelength of 1064 nm, which lies far from the UV spectral range of the linear absorption attributed to the SPR and interband transitions in MNPs and glasses. For this reason, in what follows, the contributions associated with interband transitions and radiation-induced defects will be eliminated from the analysis of the experimental results.

Fig. 4 shows the experimental dependences of the $T(z)$ measured for both glasses containing copper nanoparticles in the Z-scan scheme with an open aperture [65]. Recall that the measurements carried out in this scheme make it possible to determine the nonlinear coefficient β. Silicate glasses did not demonstrated the nonlinear absorption at applied laser intensities. It can be seen from Fig. 4 that the experimental dependences $T(z)$ exhibit specific features inherent in nonlinear absorption: the $T(z)$ decreases as the focal point is approached and reaches a minimum at Z = 0. Each point in the graphs was obtained by averaging over the values measured for 40 pulses. Some distribution of the experimental points in the graphs is caused, to some extent, by the energy instabilities and, for the most part, by the time instabilities of laser radiation.

The nonlinear coefficient β of composite materials can be determined from the relationship for the $T(z)$, which, in the case of the scheme with an open aperture, is written as [121,122]

$$T(z) = q(z)^{-1} \ln\left(1 + q(z)\right). \quad (6)$$

Here, $q(z)=\beta I(z)L_{eff}$ is the laser beam parameter, $L_{eff} = (1 - e^{-\alpha_0 L})/\alpha_0$ is the effective optical path of glass with MNPs in the sample, L is the sample thickness, and $I(z)$ is the intensity of the light passed through the sample as a function of its position along

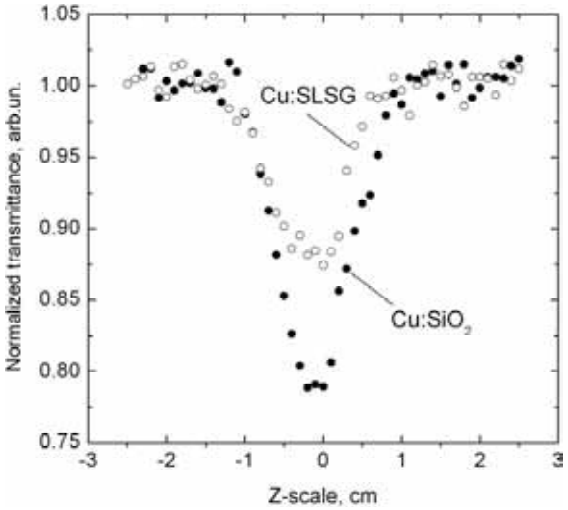

Fig. 4. Normalized transmittance as a function of the Z-position of Cu:SiO_2 and Cu:SLSG composites in the z-scan scheme with an open aperture. Samples fabricated by Cu-ion implantation with energy of 40 keV and dose of 8×10^{16} ion/cm^2. Laser intensity is 8×10^9 W/cm^2 and pulse duration is 35 ps [65].

Table 2. Nonlinear optical parameters of silicate glasses with ion-synthesised copper and silver nanoparticles measured at the wavelength of 1064 nm.

Sample	n_2,10^{-8} esu	β,10^{-6} cm/W	Re$\chi^{(3)}$,10^{-9} esu	Im$\chi^{(3)}$,10^{-9} esu	$\lvert\chi^{(3)}\rvert$,10^{-9} esu
Cu:SiO_2	-13.7	9	-32.0	6.5	3.28
Cu:SLSG	3.6	3.42	8.3	2.5	0.87
Ag:SiO_2	1.5		2.5		
Ag:SLSG	3.5		5.7		
SLSG	8.1×10^{-6}		1.4×10^{-6}		1.4×10^{-6}

the Z-axis. The parameter $q(z)$ describes the propagation of the laser beam in the material, because the following relationship holds

$$1/q(z) = 1/G(z) - 2\lambda\Delta\phi/\pi w^2 - i\lambda/\pi w^2, \quad (7)$$

where $G(z) = z[1 + z_0^2/z^2]$ is the radius of the wave front curvature in the Z-direction, $z_0 = kw^2/2$ is the diffraction length of the beam, $k = 2\pi/\lambda$ is the wave vector, $\Delta\phi = \Delta\Phi_0/(1 + z_0^2/z^2)$, $\Delta\Phi_0 = (2\pi/\lambda)n_2 I_0 L_{eff}$ - phase shift of frequency gained by the radiation passed through the sample, $w(z) = w_0(1 + z_0^2/z^2)^2$ is the beam radius at the point Z, and w_0 is the beam radius at the focal point (at a level of $1/e^2$).

At $Z = 0$ (focal plane), the parameter $q(0) = q_0$ is defined by the expression

$$q_0 = \beta I_0 L_{eff}, \quad (8)$$

where $I_0 = I(0)$ – intensity at the focal point.

Using formulas (6) and (8), it is possible to write

$$T_0 = q_0 - \ln(1 + q_0), \quad (9)$$

where T_0 is the minimum of $T(z)$ in the focal plane in the scheme with an open aperture. Expression (9) permits to determine the nonlinear absorption coefficient β. The values of β calculated in this way from the experimental data for the Cu:SiO_2 and Cu:SLSG composites are equal to 9.0×10^{-6} and 3.42×10^{-6} cm/W, respectively (Table 2).

As can be seen, the nonlinear coefficients β for these composites differ by a factor of 2.63. However, to compare correctly the coefficients β for the Cu:SiO_2 and Cu:SLSG composites, it is necessary to take into account the individual linear coefficients α_0 for layers with copper nanoparticles in different matrices ($\alpha_0^{SiO_2}$ = 9340 and α_0^{SLSG} = 5800 cm^{-1}). By assuming that the thicknesses of the layers with MNPs in the implanted glasses are virtually identical (~80 nm) [123], the nonlinear coefficient β to the linear coefficient α_0 for the relevant composite ($U = \beta/\alpha_0$) was normalized. As a result, the normalized values of $U^{SiO_2} = 9.64\cdot10^{-10}$ and $U^{SLSG} = 6.73\cdot10^{-10}$ cm^2/W, which differ by a factor of 1.432, were obtained.

To account for this discrepancy between the parameters U for different samples, proper allowance must be made not only for the difference in the linear absorption coefficients but also for the specific features in the location of the surface plasma resonance peaks attributed to copper nanoparticles. As can be seen from Fig. 3, the SPR peak assigned to MNPs is observed at 565 nm (ω_p = 17699.1 cm^{-1}) for the Cu:SiO_2 composite and at 580 nm (ω_p = 17241.4 cm^{-1}) for the Cu:SLSG composite. In such MNP systems a two-photon resonance related to the SPR can be assumed [3,11]. On the other hand, it is known that, in the range of excitations and their associated transitions in nonlinear medium, the optical nonlinearities become more pronounced with a decrease in the detuning of the frequency from the resonance (in a case, two-photon) excitation [124]. In present experiment, the frequency detuning should be treated as the difference between the SPR frequency and the frequency of two photons of the laser radiation used ω_{20} = 18797 cm^{-1} (532 nm). The difference in the location of the SPR peaks for copper nanoparticles in the SiO_2 and SLSG composites can be estimated from the following ratio:

$$M = \left(\omega_{20} - \omega_p^{Cu:SiO_2}\right)^{-1} / \left(\omega_{20} - \omega_p^{Cu:SLSG_2}\right)^{-1} = 1.42. \quad (10)$$

This value is in qualitative agreement with a ratio of 1.432 between the nonlinear coefficients β normalized to the linear coefficients α_0.

The most interesting feature in the nonlinear optical properties of glasses with copper nanoparticles irradiated at a wavelength of 1064 nm is the fact that the doubled frequency of the laser radiation is close to the SPR frequency of copper particles. This is illustrated by the diagram in Fig. 5, which shows the spectral positions of the SPR peaks of the MNPs in the samples studied and the

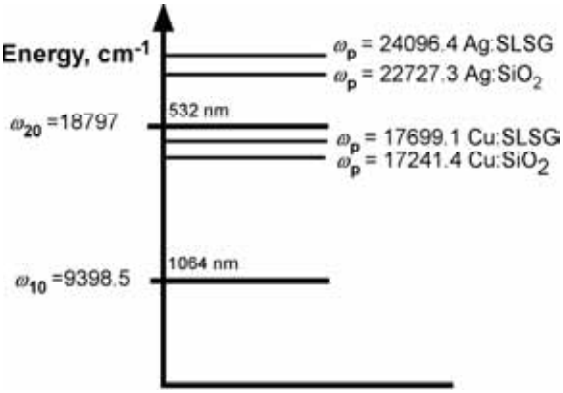

Fig. 5. Diagram of the SPR frequencies for the glasses with implanted copper and silver nanoparticles [63,64].

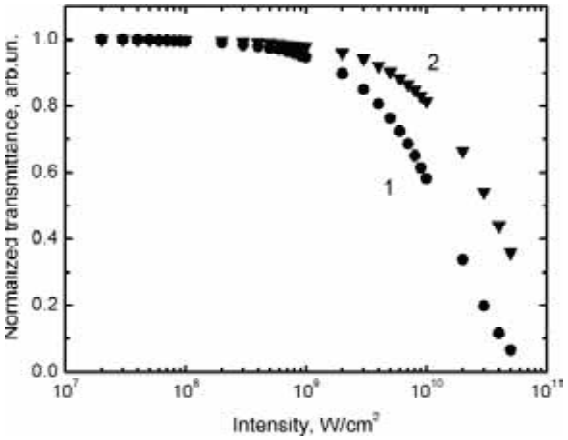

Fug. 6. Calculated curves $T(z)$ as a function of the incident radiation intensity for (1) $Cu:SiO_2$ and (2) Cu:SLSG composites [62].

spectral positions of the fundamental and doubled frequencies of the laser radiation [63,64]. Thus, from the above date, it can draw the following conclusions: (1) In the near-IR range, the large nonlinear absorption coefficients determined experimentally for glasses containing copper nanoparticles are explained by the SPR in MNPs; (2) The efficient nonlinear absorption in the composites with copper nanoparticles considered is associated with both the linear absorption of the material and the effect of two-photon resonance at the SPR frequency for copper nanoparticles, which leads to the two-photon transition at the wavelength 1064 nm.

The theoretical realization of two-photon absorption associated with the SPR of colloidal metal (silver) particles in a solution was previously discussed in [125,126], but them was difficult to analyze this possibility due to the experimental problems related to the efficient aggregation of colloidal silver under laser irradiation, which changed the nonlinear optical properties of the samples in time.

When analyzing the results presented here, it is expedient to dwell on the possible fields of practical application of the studied composites. As is known, media with nonlinear (in particular, two-photon) absorption are very promising as materials for optical limiters, which can serve, for example, for the protection of eyes and highly sensitive detectors against intense optical radiation [127]. Early, the majority of studies in this field have been performed using nanosecond laser pulses. In this case, the main mechanisms responsible for nonlinear effects are associated with the reverse saturable nonlinear absorption (fullerenes and organic and metalloorganic compounds) and nonlinear scattering (solutions of colloidal metal aggregates). Picosecond and subpicosecond laser pulses have been used only to examine the optical limiting in media belonging primarily to semiconductor materials (two-photon absorption and strong nonlinear refraction).

Since two-photon absorption at a wavelength of 1064 nm is observed in the $Cu:SiO_2$ and Cu:SLSG samples, it is of interest to investigate the optical limiting in these composites in the scheme with an open aperture. In the theoretical analysis, it was assumed that the sample is located in the region corresponding to a minimum transmittance, i.e., in the focal plane of a beam ($Z = 0$). The nonlinear absorption was studied experimentally at an operating intensity of 10^{10} W/cm^2 [62,63]. The breakdown intensity for samples containing copper nanoparticle is equal to 6×10^{10} W/cm^2. On this basis, the upper limit of the intensity for theoretical estimates was taken equal to 5×10^{10} W/cm^2. With the use of the linear and nonlinear (two-photon) absorption coefficients, the dependences of the normalized $T(z)$ on the laser radiation intensity presented in Fig. 6. It can be seen from Fig. 6 that, at the maximum intensity, the $Cu:SiO_2$ composite is characterized by an approximately fifteen-fold limiting, whereas the Cu:SLSG composite exhibits an approximately three-fold limiting. Consequently, these composites can serve as nonlinear materials for optical limiting. It is clear that the $Cu:SiO_2$ composite is more preferable from the practical standpoint. Thus, the nonlinear absorption coefficients for glasses containing copper nanoparticles were measured using the Z-scan technique and it was demonstrated that the nonlinear absorption can be associated with two-photon absorption at a wavelength

of 1064 nm. The optical limiting was analyzed for the composite materials and it was shown that the Cu:SiO_2 composite is characterized by a 15-fold limiting.

3.2. Nonlinear refraction of MNPs studied by Z-scan

Let us consider the nonlinear optical refraction of Cu:SiO_2 and Cu:SLSG composites [63,65]. Fig. 7 shows the dependences of the $T(z)$ the samples in the Z-scan scheme with a closed aperture. Each point on the plot corresponds to a value averaged over 40 pulses. A specific feature of the samples with copper nanoparticles is that the plots for different types of substrate glass demonstrate opposite signs of nonlinear refraction under the same implantation conditions. From the position of the $T(z)$ peak in the positive or negative Z-scan region (the nonlinearity sign), it can be concluded that the Cu:SiO_2 samples are characterized by self-defocusing of the laser beam ($n_2 < 0$), while the Cu:SLSG samples demonstrate a self-focusing effect ($n_2 > 0$).

To clarify the reason for the different signs of nonlinear refraction in the different glasses with copper nanoparticles, the observed self-action effects has to by analyzed. Since the wavelength of the laser radiation used in this study considerably exceeds the size of the MNPs synthesized by the implantation [6,9], the optical properties of the nanoparticles can be considered within the framework of the effective medium theory [4]. Such an approach allows to consider the composites as optically homogeneous materials, disregarding the presence of MNPs in them.

Among nonlinear optical processes contributing to the nonlinear part of the refractive index, it should be taken into account the optical Kerr effect, caused by the electronic response of atoms and molecules [124] and associated with the presence of resonance transitions in the medium [128]. The nonlinear index n_2 may vary considerably depending on the type of interaction (resonance or nonresonance). Nonresonance contributions to the n_2 of such medium as glasses are usually positive [129]. In the case of resonance interactions involving one-photon or two-photon processes, the sign of the nonlinear index n_2 is determined from the difference between the frequency of an incident electromagnetic laser wave ω_{10} (or a multiple frequency ω_{i0}) and the intrinsic resonance frequency of the material (ω_p in the case of MNPs). In particular, the nonlinear index n_2 is negative only for frequencies that are slightly below the one-photon resonances or slightly above the two-photon resonances [129].

For a homogeneous condensed medium characterized by the occurrence of resonance transitions, one can consider the standard two-level energy model [124]. Then, the corresponding equation for the nonlinear index n_2 will have the form

$$n_2 = -2\pi N \frac{|\mu_0|^4}{n_0 \eta \left(\omega_{i0} - \omega_p\right)^3}, \qquad (11)$$

where ω_p and ω_{i0} correspond to the frequencies of the SPR of MNP nanoparticles and the laser radiation, respectively; the subscript i denotes one- and two-photon processes; N is the concentration of active excitation centers considered to be dipoles (virtually equal to the number of nanoparticles in the sample); and μ_{i0} is the transition dipole moment at the frequencies ω_{i0}.

As follows from Eq. (11), N and μ_{i0} have no effect on the sign of the nonlinear index n_2 (the sign of the nonlinearity), which is determined only by the detuning from the resonance Δ_{i0}. Keeping in mind that $\chi^{(3)}$ depends linearly on n_2 [124], it can be written the relation determining the sign of the nonlinearity as

$$\operatorname{sgn} \operatorname{Re}\left[\chi^{(3)}\right] \propto -\left(\omega_{20} - \omega_p\right)^{-3} = -\operatorname{sgn} \Delta_{i0}, \qquad (12)$$

and analyze it only for the frequency ω_{20}, i.e., for the doubled frequency of the laser radiation, which lies in the vicinity of the SPR of the samples with copper particles. In other words, it is considered the effect that the frequency detuning between the sum frequencies of two laser photons and the SPR frequency exerts on nonlinear optical processes.

As was mentioned the samples show different spectral positions of the SPR maxima for MNPs in glass host matrices of different types. For example, the SPR maximum for the Cu:SLSG samples is in the vicinity of 580 nm, while the SPR peak of the Cu:SiO_2 samples lies near 565 nm. Substituting the frequencies of the SPR of copper nanoparticles in SiO_2 and SLSG (Fig. 5) and the frequency ω_{20} ~18797 cm^{-1} (the frequency of the two-photon excitation of the laser radiation used) into Eq. (12), a negative sign of the detuning is obtained, which points to a negative contribution to the nonlinear susceptibility for the matrices of both types. These conditions correspond to the self-defocusing of laser radiation, which was experimentally observed for the Cu:SiO_2 sample (Fig. 7a). Thus, the two-level model used in this paper gives the proper sign of

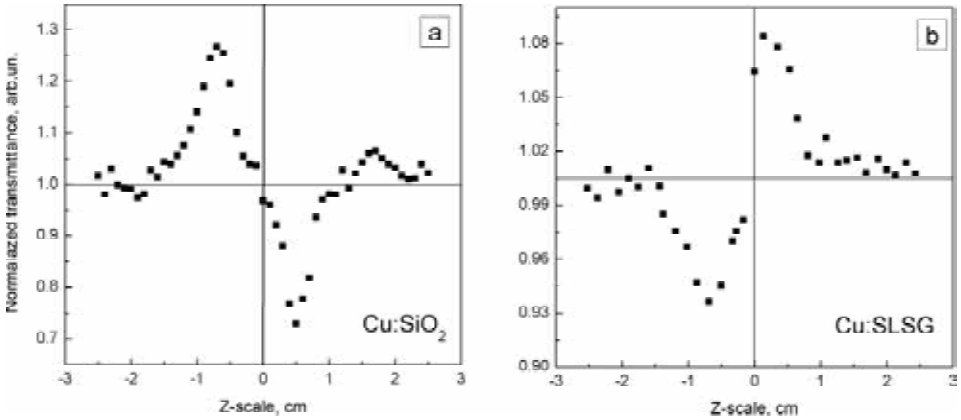

Fig. 7. Dependence of the curves $T(z)$ for (a) Cu:SiO_2 and (b) Cu:SLSG composites in the Z-scan scheme with an close aperture. Samples fabricated by Cu-ion implantation with energy of 40 keV and dose of 8×10^{16} ion/cm^2. Laser intensity is 8×10^9 W/cm^2 and pulse duration is 35 ps [65].

nonlinearity in the Cu:SiO_2 system excited by laser radiation at a frequency lying outside the SPR region of its particles, namely, at a frequency about two times lower than the SPR frequency.

A noticeable contribution to the n_2 can also be made by the thermal effect, i.e., by the heat transfer from MNPs and defects of a dielectric host matrix heated by laser radiation [130]. The rise time τ_{rise} of n_2 variations is determined by $\tau_{rise} = R_{beam}/V_s$, where R_{beam} is the beam-waist radius and V_s is the sound velocity in the lattice. In present case (R_{beam} = 75 μm, $V_s \approx$ 5500 m/s) the time necessary for both the distribution of the density of a material and its n_2 to reach their stationary values - t_{relax} ~ 13-15 ns - is three orders of magnitude longer than the pulse duration (35 ps). This allows one to exclude from consideration the influence of the thermal effect on the nonlinear optical properties of the composites at present experiment and regard the electronic optical Kerr effect as the main factor.

On the other hand, for the Cu:SLSG sample, the self-focusing of the laser radiation (Fig. 7b) was observed [63], which contradicts the conclusions derived from equation (12). To reveal the reasons for the different self-action effects in the glasses, it is necessary to consider the influence of the substrate on the nonlinear optical properties of the composites. For this purpose, the dependences of the $T(z)$ for both types of glasses without MNPs was measured. The SiO_2 substrate shows no noticeable changes in the character of the $T(z)$ under irradiation with the intensities used in this study; i.e., this glass does not demonstrate nonlinear refraction and the nonlinearities observed in the Cu:SiO_2 samples are evidently caused by the copper nanoparticles.

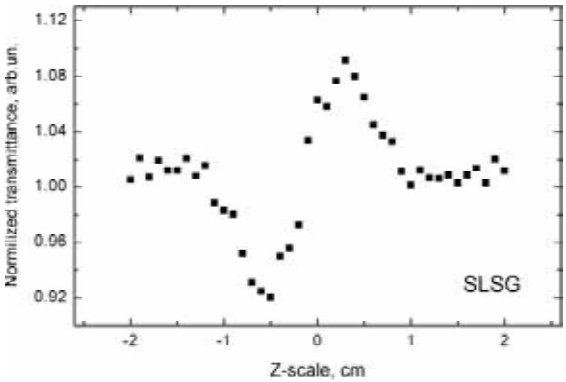

Fig. 8. Dependence of the curves $T(z)$ for SLSG in the z-scan scheme with an close aperture [63].

At the same time, the SLSG matrix exhibits a self-focusing effect (Fig. 8). To estimate the contribution of the glass substrate to the optical refraction of the Cu:SLSG sample, it was determined and compared the values of $\chi^{(3)}$ for the SLSG and Cu:SLSG samples. In the general case, when a material simultaneously exhibits both nonlinear refraction and nonlinear absorption, the nonlinear susceptibility is a complex quantity

$$\chi^{(3)} = \mathrm{Re}\left[\chi^{(3)}\right] + i\,\mathrm{Im}\left[\chi^{(3)}\right], \qquad (13)$$

where the real part is related to the nonlinear index n_2 and the imaginary part is related to the nonlinear coefficient β. As was mentioned the used glasses, contrarily to the samples with nanoparticles, have no nonlinear absorption and, hence, $\chi^{(3)}$ for the SLSG substrates is directly real-valued and can be expressed in terms of n_2 as

$$\mathrm{Re}\left[\chi^{(3)}\right] = \frac{n_0}{3\pi} n_2. \qquad (14)$$

This parameter can be experimentally estimated using the known Z-scan relations [121]

$$\Delta T_{m-v} = 0.404\left(1-S\right)^{0.25}\left|\Delta\Phi_0\right|, \qquad (15)$$

where $\Delta T_{m\text{-}v}$ is the normalized difference between the maximum and the minimum (valley) of the measured $T(z)$, S is the percent of radiation passing through the aperture and reaching the photodiode.

Applying relations (15) to the experimental data (Fig. 8) obtained for the SLSG substrate, a value of n_2 equal to 8.1×10^{-14} esu were estimated, while for the Cu:SLSG sample this parameter was detected to be of $n_2 = 3.6\times10^{-8}$ esu. The values of n_2 measured for all the samples studied are listed in the Table 2. Using relation (14) for the $Re[\chi^{(3)}]$, it was obtained that, for SLSG, which shows no nonlinear absorption, $|\chi^{(3)}|$ is equal to 1.4×10^{-14} esu, while $Re[\chi^{(3)}]$ for Cu:SLSG is equal to 8.3×10^{-9} esu (Table 2).

Taking into account that the nonlinear susceptibility in Cu:SLSG is a complex-valued parameter, whose imaginary part is expressed via the nonlinear coefficient β as

$$\mathrm{Im}\left[\chi^{(1)}\right] = \frac{n_h\varepsilon_h c^2}{\omega}\beta. \qquad (16)$$

Using Eq. (13) and the value of $\mathrm{Re}[\chi^{(3)}]$ for the given medium, then the value of the nonlinear susceptibility is $|\chi^{(3)}| = 8.7\times10^{-9}$ esu (Table 2) [63].

Since only the $\mathrm{Re}[\chi^{(3)}]$ is responsible for the nonlinear refraction in a material, it is possible to use the such nonlinear parameters (Table 2) to compare the SLSG and Cu:SLSG samples. In order to eliminate the influence of both the linear absorption and the difference in the thicknesses of the samples, in practice, one does not compare directly the values of $\mathrm{Re}[\chi^{(3)}]$, but rather their normalized values $\mathrm{Re}[\chi^{(3)}]\,L_{\mathrm{eff}}$ (in this case, L_{eff} includes a correction for the linear absorption). Using L_{eff} of the wavelength 1064 nm for the samples of both types, it is possible to get $\mathrm{Re}[\chi^{(3)}]\,L_{\mathrm{eff}} = 4.92\times10^{-14}$ esu×cm for Cu:SLSG and $\mathrm{Re}[\chi^{(3)}]\,L_{\mathrm{eff}} = 3.45\times10^{-15}$ esu×cm for SLSG. Therefore, the nonlinear parameters of pure SLSG are lower by an order of magnitude than the same parameters for the glasses containing nanoparticles.

Discussing the reasons for the self-focusing observed in the experiment (Fig. 7), i.e., the reasons for the positive contribution to the nonlinear susceptibility of Cu:SLSG, it should be take into account the considerable (~30%) linear absorption of SLSG in the spectral region of the laser radiation (Fig. 3). If a material exhibits the effect of saturation at the laser wavelength, the total absorption will decrease upon the laser irradiation. However, if a material is characterized by nonlinear absorption, the total absorption will increase, as is observed for the glasses with nanoparticles. The nonlinear absorption of Cu:SLSG causes an additional decrease in the intensity of the transmitted light in the focal plane by approximately 10–12%, while for Cu:SiO_2, whose linear absorption is ~15%, this value is equal to 18%. Irrespective of the conditions of the laser radiation which was choose here, the increase in the total absorption of Cu:SLSG can be caused by the nonlinear thermal effect predicted early [131], and observed for [132] in silicate glasses containing radio-frequency sputtered copper nanoparticles with size of 2.2±0.6 nm irradiation at the wavelength 1064 nm, when positive nonlinear susceptibility was recorded using trains of picosecond pulses (100 pulses in a train).

Consider nonlinear refraction of glass containing silver nanoparticles. The composites with silver were prepared by Ag-ion implantation into amorphous SiO_2 and soda lime silicate glasses (SLSG) as described [23]. The energies of 60 keV and dose 4×10^{16} ion/cm^2 and at a beam current density of 10 μA/cm^2 were used. The penetration depth of the MNPs in the glasses for given energy of implantation did not exceed 80 nm [123]. Optical transmittance spectra of implanted samples Ag:SiO_2 and Ag:SLSG are presented in Fig. 9. MNPs such as Ag in dielectric medium show optical absorption determined by SPR with maximum near 415 – 440 nm [4]. Fig. 10 shows the experimental dependences of the $T(z)$ of the samples Ag:SiO_2 and Ag:SLSG during Z-scanning in the scheme with a closed aperture. Similarly to the case with copper nanoparticles, the results of the measurements are the same for the laser irradiation of both sides of the sample. As follows from Fig. 10, both types of glasses with silver nanoparticles demonstrate self-focusing of laser radiation. The values n_2 and $\mathrm{Re}[\chi^{(3)}]$ are presented in Table 2. The nonlinear absorption was not detected for these samples.

Estimate the nonlinear optical contributing to both the magnitude and the sign of the nonlinear susceptibility $\chi^{(3)}$. Similarly to the case with copper nanoparticles, the spectral positions of the SPR bands in the samples with silver nanoparticles depend on the type of substrate (Fig. 9). The SPR maximum lies at about 415 nm ($\omega_p = 24096.4$ cm^{-1}) for the Ag:SiO_2 and at 440 nm ($\omega_p = 22727.3$ cm^{-1}) for the Ag:SLSG samples. As can be seen from the diagram in Fig. 5, the frequency of the sum of two photons of the laser radiation is lower than the SPR

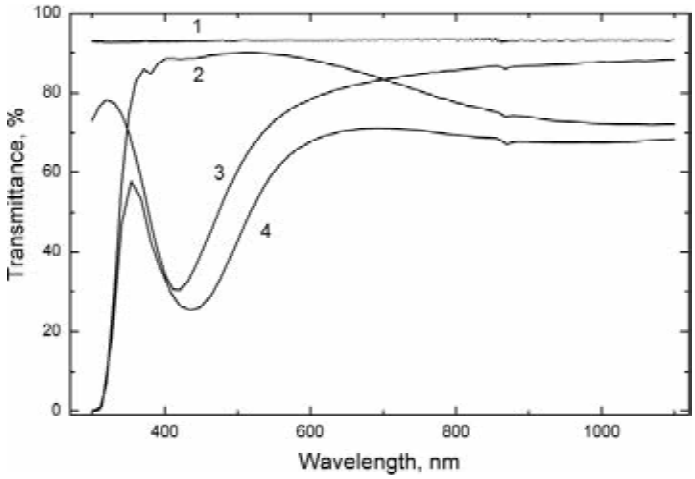

Fig. 9. Transmittance spectra of (1) SiO_2 and (2) SLSG before and after Ag-ion implantation with energy of 60 keV and dose of 4×10^{16} ion/cm^2 (3) Ag:SiO_2 and (4) Ag:SLSG [23].

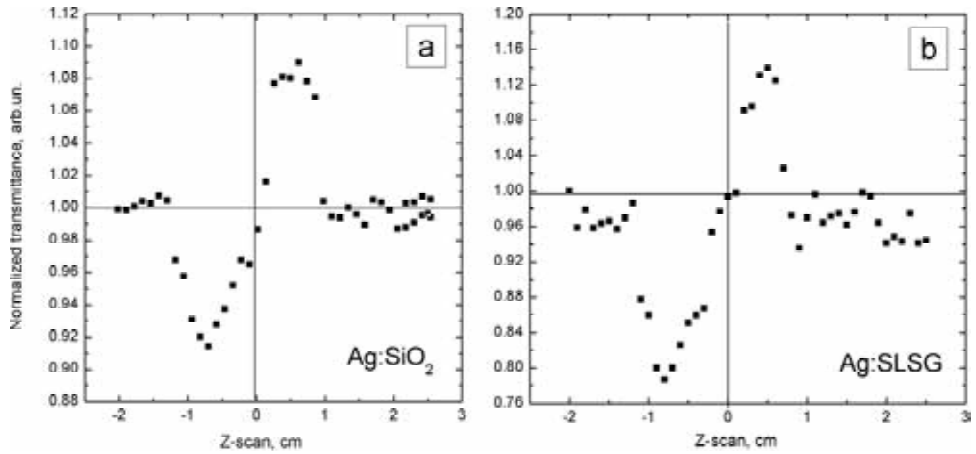

Fig. 10. Dependence of the curves $T(z)$ for (a) Ag:SiO_2 and (b) Ag:SLSG composites in the Z-scan scheme with an close aperture. Samples fabricated by Ag-ion implantation with energy of 60 keV and dose of 4×10^{16} ion/cm^2. Laser intensity is 8×10^9 W/cm^2 and pulse duration is 35 ps [63].

frequency for nanoparticles in either matrix, which corresponds to a positive sign of the detuning and, as a consequence, leads to a positive contribution to the nonlinear susceptibility. Hence, no two-photon absorption occurs in the samples with silver nanoparticles.

In practice, the efficiency of the optical switching is often evaluated by the ratio between the nonlinear (two-photon) absorption coefficient and the nonlinear refractive index at a given wavelength; the value of this critical parameter was estimated to be $K = \beta\lambda/\gamma < 1$, where γ is the nonlinear refractive index in SI units [133]. Substituting the experimentally obtained β and γ, it was that K is equal to 2.55 for Cu:SiO_2 and 3.73 for Cu:SLSG, which is considerably greater than unity. At the same time, the samples with silver nanoparticles (Ag:SiO_2 and Ag:SLSG), due to the absence of nonlinear absorption, have $K << 1$, which makes them promising for the development of optical switches at the wavelength 1064 nm. As example, It can be mentioned that the effect of the two-photon absorption on the process of optical switching was also considered in [134], where the authors studied silver-doped glasses $Ag_2As_{39}S_{59}$. It was assumed that silver particles may form in these glasses. The parameter K for that glass was found to be equal to 2.9.

3.3. RZ-scan technique

There are different approaches for the study of nonlinear optical properties of various materials, for example, degenerate four-wave mixing [135], nonlinear optical interferometry [136], Z-scan [120,121]). As was mentioned the latter technique allows de-

Table 3. Ion implantation conditions and nonlinear optical parameters of Al_2O_3 with ion-synthesized silver, copper and gold nanoparticles measured at the wavelength of 1064 nm. * - thermal annealing [30].

Sample	No.	Energy, keV	Current density, μA/cm²	Ion dose, 10^{17} ion/cm²	I_0, W/cm²	n_2, 10^{-11} cm²/W	Re[$\chi^{(3)}$], 10^{-9} esu
$Ag:Al_2O_3$	1	30	3	3.75	4.3	3.40	0.94
$Ag:Al_2O_3$	2	30	6	3.75	4.3	3.89	1.07
$Ag:Al_2O_3$	3	30	10	3.75	4.3	5.36	1.48
$Cu:Al_2O_3$	4	40	2.5	0.54	7.7	-3.75	-1.04
$Cu:Al_2O_3$	5	40	12.5	1.0	7.7	-4.96	-1.38
$Au:Al_2O_3$	6	160	10	0.6	2.3	-28.15	-7.77
$Au:Al_2O_3$	7*	160	10	0.6	2.8	-32.68	-10.0
$Au:Al_2O_3$	8	160	10	1.0	2.3	-38.76	-10.7
$Au:Al_2O_3$	9*	160	10	1.0	2.8	-44.30	-12.2

termining both the value and the sign of nonlinear optical indexes n_2 and β. There are several modifications of the Z-scan technique, such as transmission Z-scan (TZ-scan) [120,121], eclipsing Z-scan [137], two-beams [138], reflection Z-scan (RZ-scan) [139-141], time-resolved Z-scan [142], etc. The RZ-scan has an advantage with comparing to the others that allows studying the optical nonlinearities of materials with a limited optical transparency. This technique is based on the analyze of the surface properties of materials, whereas the others are used for the investigation of bulk characteristics of media. The application of RZ-scan was firstly presented in [14], where the nonlinear refraction of gallium arsenide was studied in at a wavelength of 532 nm at which this semiconductor is fully opaque. On the other hand, this technique can also be applied for transparent materials and can be used for the comparison with conventional TZ-scan.

The RZ-scan technique was firstly applied for measurement of nonlinear characteristics of low-transparency dielectric layers with MNPs beyond the region of the SPR absorption of particles [29,94]. Consider some examples with composites based on dielectric with copper, silver and gold nanoparticles synthesized by ion implantation. As a substrate for such model composites an artificial sapphire (Al_2O_3) was used. Whose surface of the sapphire opposite to the implanted surface was frosted, because of which the sample was almost nontransparent in visible and IR-spectral area. Ion implantation was performed with Ag^+, Cu^+, and Au^+ [95,143]. Experimental conditions of ion implantation used for fabrication of MNPs in Al_2O_3 are presented in Table 3 [30].

The RZ-scan setup for measurement of nonlinear refraction is presented in Fig. 11. The Nd:YAG laser (λ = 1064 nm, τ = 55 ps) operated at a 2 Hz pulse repetition rate was applied. Laser radiation was focused by a 25-cm focal length lens (1). The maximum intensity and the beam waist radius in the focal plane were measured to be $I_0 = 7 \cdot 10^9$ W/cm² and 72 μm, respectively. The sample (2) was fixed on the translation table (7) and moved along the Z-axis. The angle of incidence of laser radiation on the surface of sample was 30°. A part of radiation was reflected from the beam splitter (10) and measured by photo-diode (3) to control the energy of laser pulses. The radiation reflected from the surface of sample was directed to the mirror (10) and than collected by the lens (11) that allowed registering all the reflected radiation by photo-diode (5). To decrease the influence of the instability of laser radiation, the ratio $R(z)$ between the reflected signal and the incident one was calculated.

In the case of RZ-scan the refractive nonlinearities are measured without aperture (for

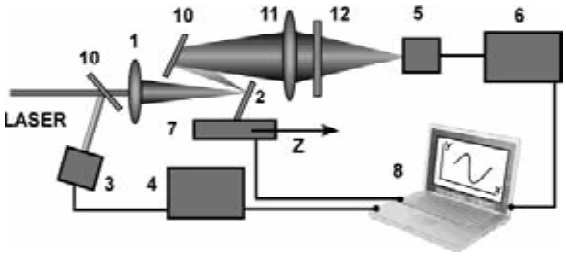

Fig. 11. Experimental RZ-scan setup for nonlinear measurements.

example, see [144]). In RZ-scan scheme, the phase changes are produced by absorptive nonlinearities and the aperture is needed in this case. The refractive nonlinearities are responsible for the amplitude changes of reflected radiation so there is no need to use an aperture before the detector. The measurements of the refractive nonlinearities of samples (that are the subject of our studies) were carried out without an aperture, thus neglecting the influence of phase changes caused by nonlinear absorption.

The principles of RZ-scan can be described as follows. The sample moves during the experiment through the focal plane of focusing lens. The amplitude and phase of reflected beam change due to the influence of nonlinear refraction and nonlinear absorption. No nonlinear effects appear when the sample is positioned far from the focal plane, so the ratio $R(z)$ of the reflected and incident laser radiation is constant. When the sample approaches focal plane, the laser intensity becomes higher and the nonlinear effects occur. In the case of positive nonlinear refraction (n_2>0), the movement of sample close to the focus leads to the growth of $R(z)$. After crossing the focal plane the nonlinear refraction diminishes that leads to a decrease of $R(z)$ down to previous value. In the case of self-defocusing (n_2<0) the opposite feature will be observed with the valley appearing in the $R(z)$ dependence. One can conclude about the sign of n_2 from the $R(z)$ dependence.

The expression for the intensity of radiation reflected from the surface of a sample can be written in the form [139-141]

$$I_R(z) = I_0 \left| \left(R_0 V_0^{-1}(z) + R_1(\theta)\left(n_2 - ik_2\right) \times I(z) V_1^{-1}(z)\left(1 - ix'\right)\right)\right|^2 . \quad (17)$$

Here, k_2 is the coefficients of nonlinear extinction; R_0 is the linear reflection coefficient, $V_m(z) = g(z) - id/d_m$, $g(z) = d/d_0 x$, d is the distance from the sample to the far-field aperture; $d_m = k\omega^2_{m0}/2$, $\omega^2_{m0} = w^2(z)/(2m + 1)$, $\omega^2(z) = \omega^2(1 + x^2)$, $x = z/z_0$, $z_0 = k\omega^2_0/2$ is the diffraction length of the beam; ω_0 is the beam waist radius; z characterizes the sample position;

$$R_l(\theta) = \frac{2n_0^3 \cos(\theta) - 4n_0 \cos(\theta)\sin^2(\theta)}{n_0^4 \cos^2(\theta) - n_0^2 + \sin^2(\theta)} \times \left[n_0^2 - \sin^2(\theta)\right]^{-1/2}, \quad (18)$$

and θ is the angle of incidence of the beam [144]. Substituting into Eq. (17) the parameters given above, it will be obtained the following expression for the normalized reflection:

$$R(z,\theta) = 1 - \frac{\left(4R_1(\theta)/R_0\right) I_0 k_2 x'}{\left(x'^2 + 9\right)\left(x'^2 + 1\right)} + \frac{\left(2R_1(\theta)/R_0\right) I_0 n_2 \left(x'^2 + 3\right)}{\left(x'^2 + 9\right)\left(x'^2 + 1\right)} + \frac{\left(R_1(\theta)/R_0\right) I_o^2 \left(n_2^2 + k_2^2\right)}{\left(x'^2 + 9\right)\left(x'^2 + 1\right)} \quad (19)$$

Here, the first expression on the right-hand side is responsible for the nonlinear absorption, the second expression describes the nonlinear refraction, and the third expression characterizes their joint effect. It should be noted that Eq. (18) was derived without taking into account the effect of thermal processes, which are characteristic of nanosecond pulses [130] or of radiation with a high pulse repetition rate [131]. To determine the real part of the third-order nonlinear susceptibility, the expression (14) was used.

For practical purpose the $R(z)$ power could be presented as follows [144]:

$$P(z) = 1 + 2\mathrm{Re}\left[R\left(n_2 + ik_2\right)\right] \times \frac{\int_0^\infty \left|E(\rho, z)\right|^4 \rho d\rho}{\int_0^\infty \left|E(\rho, z)\right|^2 \rho d\rho}, \quad (20)$$

where ρ the radial coordinates, and $E(\rho,z)$ is the incident beam amplitude.

This equation describes the general case, when both nonlinear refraction and nonlinear absorption appear simultaneously during the reflection from the sample. However, the application of open-aperture RZ-scan allowed neglecting the influence of nonlinear absorption for the measurements of nonlinear refraction [145].

3.3.1. RZ-scan study of Ag:Al_2O_3

The spectra of linear optical reflection for both initial Al_2O_3 and Ag:Al_2O_3 composites obtained by ion implantation under different conditions presented in Fig. 12. Samples 1-3 Ag:Al_2O_3 were implanted at fixed doses and energies but at different ion current densities which increases with the sample number (Table 3). The thickness of a layer containing silver nanoparticles was about 50 nm [123].

As is seen from Fig. 12, in contrast to nonimplanted Al_2O_3, all the implanted samples are characterized by the presence in the visible spectral region of a broad selective reflection band with a maximum near 460 nm, whose intensity is slightly

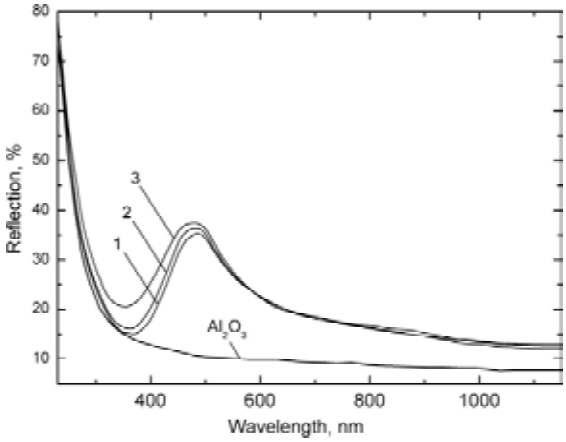

Fig. 12. Reflectance spectra of Al_2O_3 before and after Ag-ion implantation with energy of 30 keV, dose of 3.75×10^{17} ion/cm^2 and different current densities (1) 3; (2) 6 and (3) 10 μA/cm^2 [30].

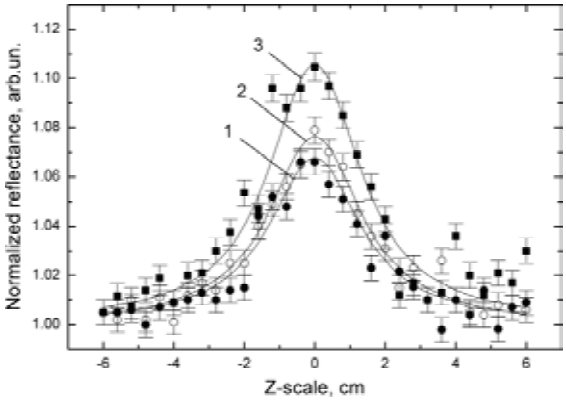

Fig. 13. Dependence of the curves $R(z)$ for Ag:Al_2O_3 composites implanted with energy of 30 keV, dose of 3.75×10^{17} ion/cm^2 and different current densities (1) 3; (2) 6 and (3) 10 μA/cm^2. Laser intensity is 4.3×10^9 W/cm^2 and pulse duration is 55 ps. Solid line is modeling [30].

higher for the samples obtained at higher ion currents. This reflection band appears due to the formation of silver nanoparticles in the implanted Al_2O_3 and corresponds to the SPR absorption in MNPs [4]. A sharp increase in the reflection intensity in the shorter wavelength region beginning from approximately 380 nm (beyond the SPR band) is caused by the absorption of light by the Al_2O_3 matrix and by interband transitions in metal NPs.

As was shown recently [146], an increase in the ion current density during the implantation of silver ions into SiO_2 leads to an increase in the portion of the metal phase (MNPs) in the sample. This is explained by an increase in the temperature of the dielectric irradiated by high ion currents and, hence, by a higher diffusion mobility of implanted silver ions and thus their more efficient incorporation into MNPs. In the general case, this may result in an increase both in the number of MNPs and in their sizes, which leads to a higher SPR absorption of MNPs. Therefore, the increase in the SPR reflection intensity in Fig. 12 should be related to a larger portion of metallic silver in Al_2O_3 implanted at higher currents. Since the spectral positions of the SPR band maxima almost do not change, hence it is possible to conclude that an increase in the ion current density under these conditions of silver implantation into Al_2O_3 results in a slight increase only in the concentration of MNPs rather than in their dimensions, which would immediately cause a spectral shift of the SPR reflection maximum.

The experimental $R(z)$ dependences for the Ag:Al_2O_3 samples measured by RZ-scanning at the wavelength 1064 nm at the laser radiation intensity $I_0 = 4.3\times10^9$ W/cm^2 are presented in Fig. 13. Dependences $R(z)$ for all the samples have the shape of a bell with the top directed upward, symmetrical with respect to $Z = 0$, and by the positive n_2. It should be noted that the tops of the bell-shaped dependences are higher for the samples implanted at higher ion currents, i.e., for the samples with a higher content of metallic silver.

Unimplanted Al_2O_3 shows no such optical nonlinearity in experiments with laser radiation intensity up to the optical breakdown. Thus, the nonlinear optical effects shown in Fig. 13 are caused by the presence of silver nanoparticles in Al_2O_3. It is also interesting that the optical nonlinearities of silver particles are observed at laser irradiation at a wavelength outside the SPR absorption of the MNPs.

Using modeled $R(z)$ dependences (Fig. 13) and fitting by them the experimental data, values of n_2 and Re[$\chi^{(3)}$] in each sample were estemated and presented in Table 3. The analysis of the results shows that the samples with a higher concentration of silver nanoparticles have higher values of n_2 and Re[$\chi^{(3)}$].

3.3.2. RZ-scan study of Cu:Al_2O_3

The second type of samples is the Al_2O_3 with copper nanoparticles. In contrast to the previous series of Ag:Al_2O_3 samples (1–3) in Table 3, in which the content of MNPs was varied by using different ion current densities, one of the samples with copper

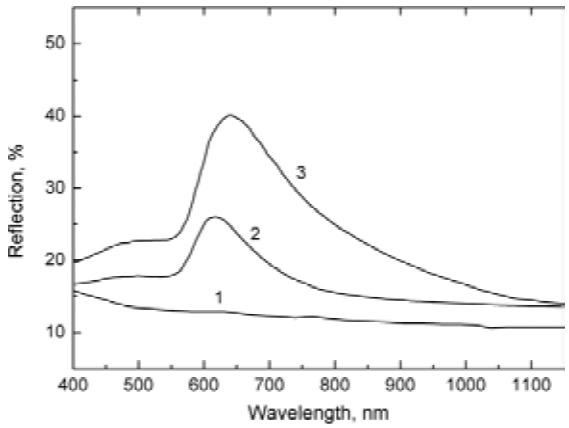

Fig. 14. Reflectance spectra of Al_2O_3 before (1) and after Cu-ion implantation with energy of 40 keV and different parameters: dose of $0.54 \cdot 10^{17}$ ions/cm^2 and 2.5 μA/cm^2 and (2) dose of 1.0×10^{17} ion/cm^2 and 12.5 μA/cm^2 (3) [147].

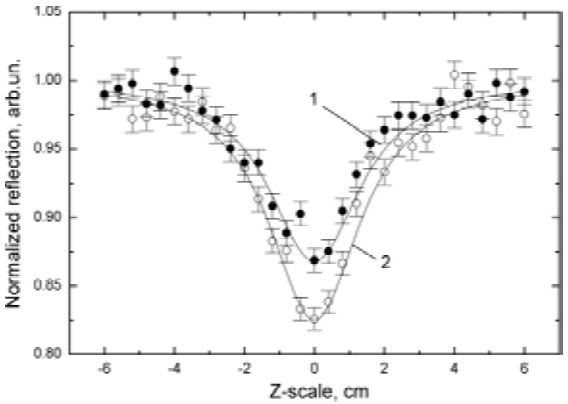

Fig. 15. Dependence of the curves $R(z)$ for Cu:Al_2O_3 composites implanted with energy of 40 keV (1) dose of $0.54 \cdot 10^{17}$ ions/cm^2 and current density 2.5 μA/cm^2 and (2) dose of 1.0×10^{17} ion/cm^2 and current density of 12.5 μA/cm^2. Laser intensity is 7.7×10^9 W/cm^2 and pulse duration is 55 ps. Solid line is modeling [30].

nanoparticles (sample 4) was obtained by implantation with a small dose ($0.54 \cdot 10^{17}$ ions/cm^2) and a low ion current (2.5 μA/cm^2), while the other sample (sample 5) was implanted at a larger dose (10^{17} ions/cm^2) and a higher current (12.5 μA/cm2). The energy of ion implantation was equal to 40 keV for both samples (Table 3).

This choice of ion implantation regimes (Table 3) in the case of copper nanoparticles allowed to obtained samples with a noticeably different filling factor of the metal phase and, in particular, with different sizes of MNPs. This is illustrated in Fig. 14, which shows the linear reflection spectra of Cu:Al_2O_3 with the SPR absorption bands of copper NPs [147], whose maxima take clearly different positions. Sample 5, which has a higher concentration of copper nanoparticles, exhibits the band at a longer wavelength (with the maximum at ~650 nm) than sample 4 (~610 nm), which points to the presence of larger MNPs in sample 5 [21,147]. A pronounced difference in the portion of the metal phase and in the size of MNPs also manifests itself in the intensity of the SPR bands. The reflection intensity for sample 5 is noticeably higher than that for sample 4.

The experimental and calculated dependences $R(z)$ for the Cu:Al_2O_3 samples are shown in Fig. 15. Since the efficiency of the electronic SPR excitation in copper nanostructures (in particular, in films, wires, *etc*.) is known to be noticeably lower than in silver particles [4], it was chosen a somewhat higher intensity of laser radiation for measuring their nonlinear optical properties $I_0 = 7.7 \cdot 10^9$ W/cm^2 (Table 3) than for Ag:Al_2O_3. The $R(z)$ dependences obtained are also bell-shaped and symmetrical with respect to the point $Z = 0$, which points to self-focusing in the Cu:Al_2O_3 samples due to the presence of copper nanoparticles. However, in contrast to the case with Ag:Al_2O_3, the tops of the bells are directed downward, which clearly testifies to the self-defocusing of the laser beam in the samples with copper nanoparticles, i.e., to a negative n_2 (Table 3). The reasons for such a different behavior of the nonlinear optical properties of Ag:Al_2O_3 and Cu:Al_2O_3 samples will be discussed below, but it should be mentioned that a difference in the signs of n_2 was also observed in transmission Z-scan measurements at the same wavelength of 1064 nm in samples of SiO_2 with silver and copper nanoparticles (previous paragraph). Estimated values of n_2 and $\mathrm{Re}[\chi^{(3)}]$ in Cu:Al_2O_3 by simulating the $R(z)$ dependences and comparing them with experimental data are presented in Table 3. It is found that the sample with a higher content of the metal phase (sample 5) has higher $|n_2|$ and $|\mathrm{Re}[\chi^{(3)}]|$.

3.3.3. RZ-scan study of Au:Al_2O_3

Samples (6–9) described in Table 3 is the Al_2O_3 containing ion-synthesized gold nanoparticles, which are also characterized by efficient SPR absorption in the visible spectral region. As in the case with copper ions, two different implantation doses, $0.6 \cdot 10^{17}$ and $0.1 \cdot 10^{17}$ ions/cm^2, but higher irradia-

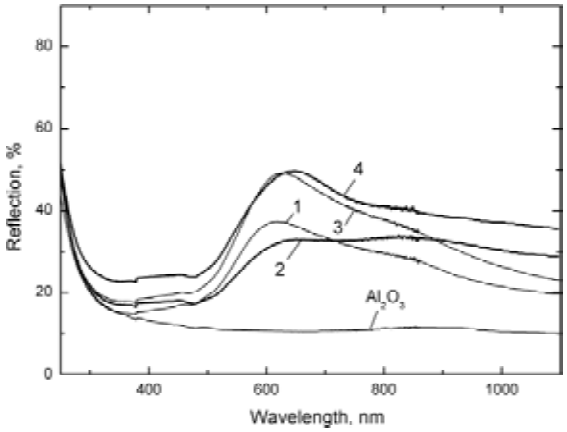

Fig. 16. Reflectance spectra of Al_2O_3 before and after Au-ion implantation with energy of 160 keV, current density of 10 μA/cm^2 with different doses of $0.6 \cdot 10^{17}$ ions/cm^2 (3,4) and 1.0×10^{17} ion/cm^2 (1,2). Samples annealed after ion implantation during 1 h at temperature of 800 °C (2,4) [94,95].

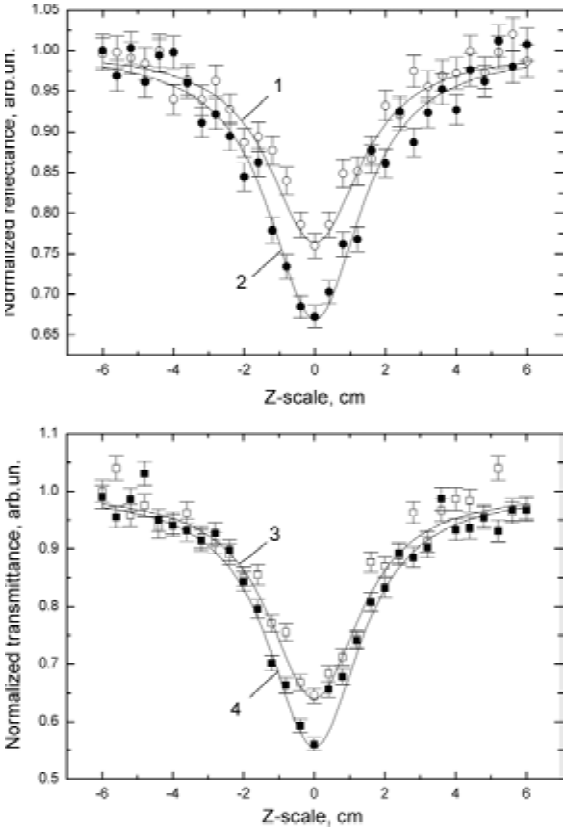

Fig. 17. Dependence of the curves $R(z)$ for Au:Al_2O_3 composites implanted with energy of 160 keV with doses $0.6 \cdot 10^{17}$ ions/cm^2 (1,2) and 1.0×10^{17} ion/cm^2 (3, 4) at current density of 10 mA/cm^2 with different doses of $0.6 \cdot 10^{17}$ ions/cm^2 (3,4) and 1.0×10^{17} ion/cm^2 (1,2). Samples created by ion implantation (1,3) and samples created by ion implantation with subsequent thermal annealing during 1 h at temperature of 800 °C (2,4). Laser intensity is 2.3×10^9 W/cm^2 and pulse duration is 55 ps. Solid line is modeling [94,95].

tion energies, 160 keV (samples 6 and 8, Table 3) [94,95]. Since, at such high energies, the implanted impurity accumulates in a thicker subsurface layer of the dielectric irradiated [123], the impurity concentration necessary for the nucleation of MNPs accumulates over a longer time. In order to increase the size of MNPs, some of samples 7 and 9 were annealed in a furnace for 1 h at a temperature of 800 °C (Table 3) [94,95].

The spectra of linear optical reflection from the Au:Al_2O_3 samples 6–9 are presented in Fig. 16. The formation of gold nanoparticles by ion implantation is proved by the presence of SPR reflection bands peaked at about 610 nm. Comparing samples 6 and 8 (curves 1 and 3, Fig. 16), obtained directly by ion implantation, it is possible to see that an increase in the implantation dose (sample 8) results in a slight shift of the maximum of the SPR reflection (to ~620 nm), which is accompanied by a noticeable increase in the intensity. This fact, as in the previous case with the implantation with copper ions (samples 4 and 5), points to a higher filling factor of the metal phase in sample 8 Au:Al_2O_3. Subsequent thermal treatment of these samples almost does not change the positions of the maxima of the SPR bands but leads to a sharp increase in the reflection in the long-wavelength spectral range. A broad reflection shoulder (sample 9, curve 4 in Fig. 16) or even an additional maximum (sample 7, curve 2 in Fig. 16) appearing near the SPR reflection bands can be associated with redistribution of the metal phase in the dielectric volume due to the high temperature of the material and, hence, with the formation of aggregates of MNPs. Similar spectral behavior was observed in experiments with fractal aggregates of silver particles but in solutions [148].

At present, there are no data in the literature on the nonlinear optical properties of gold nanoparticles in a solid matrix in the near-IR region (1064 nm). The first experimental results for Au:Al_2O_3 were given in [94,95] and presented in Fig. 17. Fig. 17a shows the curves for samples 6 and 7, which were obtained directly by ion implantation, while Fig. 17b presents the dependences for samples 8 and 9, obtained by ion implantation and subsequent thermal treatment. As is seen, the $R(z)$ dependences have a bell-like

shape symmetrical with respect to the point $Z = 0$, with the tops directed downward. Thus, samples (6-9) are characterized by self-defocusing, which corresponds to a negative n_2 and Re[$\chi^{(3)}$] which values presented in Table 3.

3.3.4. Nonlinear refraction of MNPs studied by RZ-scan

For the samples based on Al_2O_3, the frequencies ω_p are equal to 22222 cm^{-1} (~450 nm, Fig. 12) for silver nanoparticles, 16393–15384 cm^{-1} (~610-650 nm, Fig. 14) for cupper nanoparticles, and 16129 cm^{-1} (~620 nm, Fig. 16) for gold nanoparticles. Consider relation (12) for the case of a one-photon process (i = 1), i.e., for the frequency ω_{10} = 9398 cm^{-1} (λ = 1064 nm), which is the fundamental frequency of the laser radiation used. Substituting the values of ω_{10} and ω_p into relation (12), positive values of Re[$\chi^{(3)}$] and a negative detuning Δ_{10} for all the samples can be obtained. The positive Re[$\chi^{(3)}$] and n_2 correspond to the self-focusing of the laser radiation in the sample, which was observed experimentally for the Ag:Al_2O_3 samples (samples 1–3, Table 3).

On the other hand, the positive values of the signs of Re[$\chi^{(3)}$] and n_2 contradict the self-defocusing experimentally detected in the samples with cupper and gold nanoparticles (Figs. 15 and 17). Hence, the description of nonlinear processes in the approximation of one-photon excitation for the Cu:Al_2O_3 and Au:Al_2O_3 systems is incorrect. Therefore, consider the case of two-photon excitation for all the composite systems studied using again expression (12) but with the doubled frequency of the laser radiation, ω_{20} = 18797 cm^{-1} (λ = 532 nm). This frequency lies in the vicinity of the SPR frequencies of MNPs in Cu:Al_2O_3 and Au:Al_2O_3. Determine the signs of Δ_{20} for composites and see how they correlate with the nonlinear optical processes observed experimentally. In this case, the signs of Re[$\chi^{(3)}$] for the Cu:Al_2O_3 and Au:Al_2O_3 systems are negative, which agrees with the self-defocusing detected in experiments and suggests the occurrence of two-photon absorption in these samples. For the Ag:Al_2O_3 samples, this sign turns out to be positive again, as in the case of one-photon excitation, and correlates with the self-focusing observed in experiments. However, for silver nanoparticles in Al_2O_3, it is difficult to choose between the one-photon and two-photon excitation mechanisms. Probably, the two mechanisms are simultaneously realized in this type of MNPs and their manifestation depends on the dominant frequency of laser excitation. Thus, the two-level model correctly predicts the sign of the nonlinearity in the Cu:Al_2O_3 and Au:Al_2O_3 systems in the case of excitation by laser radiation at a frequency divisible by the doubled SPR frequency.

As was mention in the general case, a change in n_2 of a composite material can be caused by the thermal effect due to heat transfer from MNPs or defects of the dielectric host matrix heated by laser radiation [130]. Despite the duration of laser pulses used was rather short (τ = 55 ns), the influence of the thermal effect on the nonlinear refraction can be analyzed. Estimate how large a change in the refractive index of crystalline sapphire $\Delta n_{Al_2O_3}$ caused by heating can be.

The change in the refractive index due to the thermal effect can be represented in the form [130]

$$\Delta n(r,z,t) = \frac{1}{C_h \rho_h}\frac{dn}{dT}\Delta E(r,z,t), \qquad (21)$$

where C_h and ρ_h are, respectively, the heat capacity and the density of the host matrix with MNPs (in the case of sapphire, C_h = 0.419 J/g×K and ρ_h = 3.97 g/cm^3); dn/dT is the thermo-optic coefficient, equal to 13.7×10^{-6} 1/K; and $\Delta E(r, z, t)$ is the energy of the radiation absorbed in a unit volume of the material over a time t. The thermo-optic coefficient for sapphire is positive, and, hence, the thermal effect should lead to the self-focusing of laser radiation in all the samples.

Since the self-focusing of laser radiation was experimentally observed only for the samples with silver nanoparticles the thermal effect for such samples were analyzed using present experimental conditions of nonlinear measurements [94,95]. Thus, in the case of Ag:Al_2O_3, the energy of the absorbed radiation is 3.87×10^{-6} J. For the layer with silver nanoparticles of 50 nm thickness and the beam waist radius 72 mm, the analysing volume is 4.88×10^{-10} cm^3. In this case, the energy $\Delta E(r, z, t)$ is 7.92×10^3 J/cm^3. Substituting these values into Eq. (21), the value of $\Delta n(r,z,t)$H"6.53×10^{-2} will be obtained. In same time, the experimental values are from 4.33×10^{-2} to 6.83×10^{-2}. Hence, the thermal effect may manifest itself in the case of samples with silver nanoparticles. However, as it was mentioned the time τ_{rize} necessary for a change in the medium density and a corresponding change in the refractive index is determined by the ratio of the beam waist radius to the speed of sound. Taking into account our experimental conditions (ω_0 = 72 μm at the wavelength 1064 nm and V_s ~ 5000-5500 m/s), $\tau_{rize} \approx$ 13-15 ns will be again estimated. This time is three orders of magnitude longer than the pulse

duration used (55 ps), and, hence, the thermal effect caused by the propagation of an acoustic wave can be excluded from consideration in our case.

In conclusion, RZ-scan method is suited for study of nonlinear refraction of samples based on dielectrics with MNPs. Although the sensitivity of the RZ-scan method is slightly lower than that of the classical transmission Z-scan, the RZ-scan method allows one to extend the spectral range of study to the region of low transparency of composite materials. The sign of the $Re[\chi^{(3)}]$ is analyzed on the basis of the two-level model, and it is shown that $Re[\chi^{(3)}]$ of the samples with copper and gold nanoparticles are determined by the two-photon process. It is difficult to make similar conclusion for samples with silver nanoparticles.

ACKNOWLEDGEMENTS

I wish to thank my partners and co-authors from different countries D. Hole, P.D. Townsend, I.B. Khaibullin, V.I. Nuzhdin, V.F. Valeev, Yu.N. Osin, R.A. Ganeev, A.I. Ryasnyanskiy, T. Usmanov, M.K. Kodirov, V.N. Popok, and U. Kreibig. Also, I grateful to the Alexander von Humboldt Foundation and the DAAD in Germany, Austrian Scientific Foundation in the frame of Lisa Meitner Fellowship and the Royal Society in UK for financial support. This work was also supported by the Ministry of Education and Science of the Russian Federation (FTP "Scientific and scientific-pedagogical personnel of the innovative Russia" No. 02.740.11.0779).

REFERENCES

[1] J. Z. Zhang, *Optical properties and spectroscopy of nanomaterials* (Wold Sci. Pub.: London, 2009).

[2] *Optical properties of nanostructured random media*, ed. by V.M. Shalaev (Springer: Berlin, 2002).

[3] C. Flytzanis, F. Hache, M.C. Klein, D. Ricard and P. Rousignol, *Nonlinear optics in composite materials* (Elsevier Science, Amsterdam, 1991).

[4] U. Kreibig and M. Vollmer, *Optical properties of metal clusters* (Springer: Berlin, 1995).

[5] A.L. Stepanov, In: *High-power and Femtosecond Lasers*, ed. by P.-H. Barret, P.-H. and M. Palmer (NOVA Sci. Publ. Inc.: New York, 2009), p. 27.

[6] P.T. Townsend, P.J. Chandler and L. Zhang, *Optical effects of ion implantation* (Cambridge Univ. Press: Cambridge, 1994).

[7] A.L. Stepanov, In: *Metal-polymer nanocomposites*, ed. L. Nicolais and G. Carotenuto (John Wiley & Sons Publ: London, 2004) p. 241.

[8] F. Gonella and P. Mazzoldi, In: *Handbook of nanostructured materials and nanotechnology*, ed. by H.S. Nalwa (Academic Press, 2000).

[9] A.L. Stepanov, *Ion-synthesis of metal nanoparticles and their optical properties* (NOVA Sci. Publ. Inc.: New York, 2011).

[10] D. Ricard, P. Roussignol and C. Flytzanis // *Opt. Lett.* **10** (1985) 511.

[11] R.F. Haglund Jr., In: *Handbook of optical properties. Vol. II. Optics of small particles, interfaces, and surfaces*, ed. by RF. Hummel and P. Wismann (CRC Press: London, 1997), p.198.

[12] R.F. Haglund Jr., D.H. Osbone, R.H. Magruder III, C.W. White, R.A. Zuhr, D.E. Hole and P.D. Townsend, In: *Proc. Conf. Science and technology of atomically engineered materials*, ed. P. Jena, S.N. Khanna and B.K. Rao (World Sci.: Singapure, 1995), p.411.

[13] J. von Neumann, In: *Fundamentals of photonics*, eds. by B.E.A. Saleh and M.C. Teich (Wiley: New York, 2001), p. 856.

[14] J. Davenas, A. Perez, P. Thevenard and C.H.S. Dupuy // *Phys. Stat. Sol. A* **19** (1973) 679.

[15] M. Treilleux, P. Thevenard, G. Ghassagne and L.H. Hobbs // *Phys. Stat. Sol. A* **48** (1978) 425.

[16] G.W. Arnold // *J. Appl. Phys*. **46** (1975) 4466.

[17] G.W. Arnold and J.A. Borders // *J. Appl. Phys*. **48** (1977) 1488.

[18] P. Mazzoldi, G.W. Arnold, G. Battaglin, R. Bertoncello and F. Gonella // *Nucl. Instr. Meth. Phys. Res. B* **91** (1994) 478.

[19] P. Mazzoldi, G.W. Arnold, G. Battaglin, F. Gonella and R.F. Haglund Jr. // *J. Nonlinear Opt. Phys. Mater*. **5** (1996) 285.

[20] P. Chakrabotry // *J. Mater. Sci*. **33** (1998) 2235.

[21] A. Stepanov and I.B. Khaibullin // *Rev. Adv. Mater. Sci.* **9** (205) 109.

[22] A. Meldrum, R. Lopez, R.H. Magruder III, L.A. Boatner and C.W. White, In: *Material science with ion beam*, ed. by H. Barnes (Springer: Berlin, 2010).

[23] A. Stepanov // *Rev. Adv. Mater. Sci.* **26** (2010) 1.

[24] R.A. Ganeev // *J. Opt. A.: Pure Appl. Opt.* **7** (2005) 717.

[25] R.A. Ganeev and T. Usmanov // *Quant. Electr*. **37** (2007) 605.
[26] E. Cattarruzza, F. Gonella, G. Mattei, P. Mazzoldi, D. Gatteschi, S. Sangregorio, M. Falconieri, G. Salvetti and G. Battaglin // *Appl. Phys. Lett*. **73** (1998) 1176.
[27] M. Falconieri, G. Salvetti, E. Cattarruzza, F. Gonella, G. Mattei, P. Mazzoldi, M. Piovesan, G. Battaglin and R. Polloni // *Appl. Phys. Lett*. **73** (1998) 288.
[28] E. Cattarruzza, G. Battaglin, F. Gonella, R. Polloni, G. Mattei, C. Maurizio, P. Mazzoldi, C. Sada, M. Montagna, C. Tosello and M. Ferrari // *Phil. Mag. B* **82** (2002) 735.
[29] R. Ganeev, A.I. Ryasnyanskiy, A.L. Stepanov, C. Marques, R.C. da Silva and E. Alves // *Opt. Comm*. **253** (2005) 205.
[30] R. Ganeev, A.I. Ryasnyanskiy, A.L. Stepanov, T. Usmanov, C. Marques, R.C. da Silva and E. Alves // *Opt. Spectr*. **101** (2006) 615.
[31] A.I. Ryasnyanskiy // *Nonlin. Opt. Quant. Opt.* **33** (2005) 17.
[32] O. Plaksin, Y. Takeda, H. Amekura, N. Kishimoto and S. Plaksin // *J. Appl. Phys.* **103** (2008) 114302.
[33] A.I. Ryasnyansky, B. Palpant, S. Debrus, R.I. Khaibullin and A.L. Stepanov // *J. Opt. Soc. Am. B* **23** (2006) 1348.
[34] Y. Takeda, C.G. Lee and N. Kishimoto // *Nucl. Instr. Meth. Phys. Res. B* **191** (2002) 422.
[35] Y. Takeda, C.G. Lee, V.V. Bandourko and N. Kishimoto // *Proc. SPIE* **4628** (2002) 46.
[36] Y. Takeda, V.V. Bandourko, C.-G. Lee and N. Kishimoto // *Mater. Trans*. **43** (2002) 1057.
[37] N. Kishimoto, Y. Takeda, N. Umeda, N. Okubo and R.G. Faulkner // *Nucl. Instr. Meth. Phys. Res. B* **206** (2003) 643.
[38] O.A. Plaksin, Y. Takeda, K. Kono, N. Umeda, Y. Fudamoto and N. Kishimoto // *Mat. Sci. Eng. B* **120** (2005) 84.
[39] O.A. Plaksin and N. Kishimoto // *Phys. Solid State* **48** (2006) 1933.
[40] N. Kishimoto, Y. Takeda, N. Umeda, T. Gritsyna, C.-G. Lee and T. Saito // *Nucl. Instr. Meth. Phys. Res. B* **166-167** (2000) 840.
[41] Y. Takeda, N. Umeda, V.T. Gritsyna and N. Kishimoto // *Nucl. Instr. Meth. Phys. Res. B* **175-177** (2001) 463.
[42] K. Becker, L.Yang, R.F. Haglund Jr., R.H. Magruder III, R.A. Weeks and R.A. Zuhr // *Nucl. Instr. Meth. Phys. Res. B* **59-60** (1991) 1304.
[43] R.F. Haglund Jr., R.H. Magruder III, S.H. Morgen, D.O. Henderson, R.A. Weller, L. Yang and R.A. Zuhr // *Nucl. Instr. Meth. Phys. Res. B* **65** (1992) 405.
[44] R.F. Haglund Jr., L.Yang, R.H. Magruder III, J.E. Wittig, K. Becker and R.A. Zuhr // *Opt. Lett.* **18** (1993) 373.
[45] R.F. Haglund Jr., L.Yang, R.H. Magruder III, C.W. Wittig, R.A. Zuhr, L. Yang, R. Dorsinville and R.R. Alfano // *Nucl. Instr. Meth. Phys. Res. B* **91** (1994) 493.
[46] R.F. Haglund Jr. // *Mat. Sci. Eng. A* **253** (1998) 275.
[47] R.H. Magruder III, R.F. Haglund Jr., L.Yang, J.E. Wittig and R.A. Zuhr // *J. Appl. Phys.* **76** (1994) 708.
[48] L. Yang, K. Becker, F.M. Smith, R.H. Magruder III, R.F. Haglund Jr., L.Yang, R. Dorsinville, R.R. Alfano and R.A. Zuhr // *J. Opt. Soc. Am. B* **11** (1994) 457.
[49] L. Yang, D.H. Osbone, R.F. Haglund Jr., R.H. Magruder III, C.W. Wittig, R.A. Zuhr and H. Hosono // *Appl. Phys. A* **62** (1996) 403.
[50] D. Ila, E.K. Williams, S. Sarkisov, C.C. Smith, D.B. Poker and D.K. Hensley // *Nucl. Instr. Meth. Phys. Res. B* **141** (1998) 289.
[51] S. Sarkisov, E.K. Williams, M. Curley, D. Ila, P. Venkateswarlu, D.B. Poker and D.K. Hensley // *Nucl. Instr. Meth. Phys. Res. B* **141** (1998) 294.
[52] Y. Takeda, V.T. Gritsyna, N. Umeda, C.G. Lee and N. Kishimoto // *Nucl. Instr. Meth. Phys. Res. B* **148** (1999) 1029.
[53] Y. Takeda, J.P. Zhao, C.G. Lee, V.T. Gritsyna and N. Kishimoto // *Nucl. Instr. Meth. Phys. Res. B* **166-167** (2000) 877.
[54] J. Olivares, J. Requejo-Isidro, R. del Coso, R. de Nalda, J. Solis, C.N. Afonso, A.L. Stepanov, D. Hole, P.D. Townsend and A. Naudon // *J. Appl. Phys*. **90** (2001) 1064.
[55] Y. Takeda, C.G. Lee and N. Kishimoto // *Nucl. Instr. Meth. Phys. Res. B* **190** (2002) 797.
[56] Y. Takeda, J. Lu, O.A. Plaksin, H. Amekura, K. Kono and N. Kishimoto // *Nucl. Instr. Meth. Phys. Res. B* **219-220** (2004) 737.
[57] Y. Takeda, J. Lu, N. Okubo, O.A. Plaksin, T. Suga and N. Kishimoto // *Vacuum* **74** (2004) 717.
[58] R. Ganeev, A.I. Ryasnyanskiy, A.L. Stepanov and T. Usmanov // *Phys. Stat. Sol. B* **238** (2003) R5.

[59] R. Ganeev, A.I. Ryasnyanskiy, A.L. Stepanov and T. Usmanov // *Phys. Solid State* **46** (2004) 351.
[60] R. Ganeev, A.I. Ryasnyanskiy, A.L. Stepanov and T. Usmanov // *Quant. Electr.* **33** (2003) 1081.
[61] R. Ganeev, A.I. Ryasnyanskiy, A.L. Stepanov and T. Usmanov // *Phys. Stat*. Sol. B **241** (2004) R1.
[62] R. Ganeev, A.I. Ryasnyanskiy, A.L. Stepanov and T. Usmanov // *Phys. Solid* State **45** (2003) 1355.
[63] R. Ganeev, A.I. Ryasnyanskiy, A.L. Stepanov, M.K. Kodirov and T. Usmanov // *Opt. Spectr.* **95** (2003) 967.
[64] R. Ganeev, A.I. Ryasnyanskiy, A.L. Stepanov and T. Usmanov // *Phys. Stat. Sol. B* **241** (2004) 935.
[65] A.L. Stepanov, R. Ganeev, A.I. Ryasnyanskiy and T. Usmanov // *Nucl. Instr. Meth. Phys. Res. B* **206** (2003) 624.
[66] Y. Takeda, O.A. Plaksin, K. Kono and N. Kishimoto // *Surf. Coat.Technol*. **196** (2005) 30.
[67] F. Ren, C.Z. Jiang, Y.H. Wang, Q.Q. Wang and J.B. Wang // *Nucl. Instr. Meth. Phys. Res. B* **245** (2006) 427.
[68] Y.H. Wang, C.Z. Jiang, F. Ren, Q.Q. Wang, D.J. Chen and D.J. Fu // *Physica E* **33** (2006) 427.
[69] Y.H. Wang, F. Ren, Q.Q. Wang, D.J. Chen, D.J. Fu and C.Z. Jiang // *Phys. Lett. A* **357** (2006) 364.
[70] B. Ghosh, P. Chakraborty, S. Mohapartra, P.A. Kurian, C. Vijayan, P.C. Deshmukh and P. Mazzoldi // *Mat. Lett.* **61** (2007) 4512.
[71] B. Ghosh, P. Chakraborty, B.P. Singh and T. Kundu // *Appl. Surf. Sci.* **256** (2009) 389.
[72] C. Torres-Torres, J.R. Reyes-Esqueda, J.C. Cheng-Wong, A. Crespo-Sosa, L. Rodriguez-Fernandez and A. Oliver // *J. Appl. Phys*. **104** (2008) 14306.
[73] Y.H. Wang, Y.M. Wang, J.D. Lu, L.L. Ji, R.G. Zang and R.W. Wang // *Physica B* **404** (2009) 4295.
[74] Y.H. Wang, Y.M. Wang, J.D. Lu, L.L. Ji, R.G. Zang and R.W. Wang // *Opt. Comm.* **283** (2010) 486.
[75] Y.H. Wang, Y.M. Wang, C.J. Han, J.D. Lu and L.L. Ji // *Physica B* **405** (2010) 2664.
[76] Y. Takeda, J. Lu, O.A. Plaksin, K. Kono, H. Amekura and N. Kishimoto // *Thin Solid Films* **464-456** (2004) 483.
[77] Y. Takeda, O.A. Plaksin, J. Lu, K. Kono, H. Amekura and N. Kishimoto // *Nucl. Instr. Meth. Phys. Res. B* **250** (2006) 372.
[78] A. Cetin, R. Kibar, M. Hatipoglu, Y. Karabulut and N. Can // *Physica B* **405** (2010) 2323.
[79] A.L. Stepanov, R.I. Khaibullin, N. Can, R.A. Ganeev, A.I. Ryasnyanski, C. Buchal and S. Uysal // *Tech. Phys. Lett.* **30** (2004) 846.
[80] A.I. Ryasnyanskiy, B. Palpant, S. Debrus, R. Ganeev, A.L. Stepanov, N. Can, C. Buchal and S. Uysal // *Appl. Opt.* **44** (2005) 2839.
[81] A.I. Ryasnyanskiy // *J. Appl. Spect.* **72** (2005) 712.
[82] E.K. Williams, D. Ila, A. Darwish, D.B. Poker, S.S. Sarkisov, M.J. Curley, J.-C. Wang, V.L. Svetchinkov and H.W. Zandbergen // *Nucl. Instr. Meth. Phys. Res. B* **148** (1999) 1074.
[83] S.S. Sarkisov, M.J. Curley, E.K. Williams, D. Ila, V.L. Svetchinkov, H.W. Zandbergen, G.A. Zykov, C. Banks, J.-C. Wang, D.B. Poker and D.K. Hensley // *Nucl. Instr. Meth. Phys. Res. B* **166-167** (2000) 750.
[84] R. Ganeev, A.I. Ryasnyanskiy, A.L. Stepanov and T. Usmanov // *Opt. Quant. Electron.* **36** (2004) 949.
[85] A.L. Stepanov, In: *Silver nanoparticles*, ed. by D.P. Perez (In-tech: Vukovar, 2010), p. 93.
[86] B. Joseph, C.S. Suchand Sandeep, B.R. Sekhar, D.P. Mahapatra and R. Philip // *Nucl. Instr. Meth. Phys. Res. B* **265** (2007) 631.
[87] R. Rangel-Roja, J. McCarthy, H.T. Bookey, A.K. Kar, L. Rodriguez-Fernandez, J.C. Cheang-Wong, A. Crespo-Soso, A. Lopez-Suarez, A. Oliver, V. Rodriguez-Iglesias and H.G. Silva-Pereryra // *Opt. Comm*. **282** (2009) 1909.
[88] R. Rangel-Roja, J.A. Reyes-Esqueda, C. Torres-Torres, A. Oliver, L. Rodriguez-Fernandez, A. Crespo-Soso, J.C. Cheang-Wong, J. McCarthy, H.T. Bookey and A.K. Kar, In: *Silver nanoparticles*, ed. by D.P. Perez (In-tech: Vukovar, 2010), p. 35.
[89] Y.H. Wang, S.J. Peng, J.D. Lu, R.W. Wang, Y.G. Cheng and Y.I. Mao // *Vacuum* **83** (2009) 412.
[90] Y. Takeda, T. Hioki, T. Motohiro and S. Noda // *Appl. Phys. Lett.* **63** (1993) 3420.
[91] Y. Takeda, T. Hioki, T. Motohiro, S. Noda and T. Kurauchi // *Nucl. Instr. Meth. Phys. Res. B* **91** (1994) 515.
[92] Y. Takeda and N. Kishimoto // *Nucl. Instr. Meth. Phys. Res. B* **206** (2003) 620.

[93] C.W. White, D.K. Thomas, D.K. Hensley, R.A. Zuhr, J.C. McCallum, A. Pogany, R.F. Haglund Jr., R.H. Magruder III and L. Yang // *Nanostruct. Mat.* **3** (1993) 447.
[94] A.L. Stepanov, C. Marques, E. Alves, R.C. da Silva, M.R. Silva, R. Ganeev, A.I. Ryasnyanskiy and T. Usmanov // *Tech. Phys. Lett.* **31** (2005) 702.
[95] A.L. Stepanov, C. Marques, E. Alves, R.C. da Silva, M.R. Silva, R. Ganeev and A.I. Ryasnyanskiy // *Tech. Phys.* **51** (2006) 1474.
[96] Y. Takeda, O.A. Plaksin, H. Wang, K. Kono, N. Umeda and N. Kishimoto // *Opt. Rev.* **13** (2006) 231.
[97] Y. Takeda, O.A. Plaksin, H. Wang and N. Kishimoto // *Nucl. Instr. Meth. Phys. Res. B* **257** (2007) 47.
[98] R.H. Magruder III, L. Yang, R.F. Haglund Jr., C.W. White, L. Yang, R. Dorsinville and R.R. Alfano // *Appl. Phys. Lett.* **62** (1963) 1730.
[99] C.W. White, D.Z. Zhou, J.D. Budai, R.A. Zhur, R.H. Magruder III and D.H. Osbone // *Mat. Res. Soc. Proc.* **316** (1994) 499.
[100] K. Fukumi, A. Chayahara, K. Kadono, T. Sakaguchi, Y. Horino, M. Miya, K. Fujii, J. Hayakawa and M. Satou // *Jpn. J. Appl. Phys.* **30** (1991) L742.
[101] K. Fukumi, A. Chayahara, K. Kadono, T. Sakaguchi, Y. Horino, M. Miya, K. Fujii, J. Hayakawa and M. Satou // *J. Appl. Phys.* **75** (1994) 3075.
[102] N.N. Lepeshkin, W. Kim, V.P. Safonov, J.G. Zhu, R.L. Armstrong, C.W. White, R.A. Zuhr and V.M. Shalaev // *J. Nonlin. Opt. Phys. Mat.* **8** (1999) 191.
[103] V.P. Safonov, J.G. Zhu, N.N. Lepeshkin, R.L. Armstrong, V.M. Shalaev, Z.C. Ying, C.W. White and R.A. Zuhr // *Proc. SPIE* **3788** (1999) 34-41.
[104] Y. Takeda, O.A. Plaksin and N. Kishimoto // *Opt. Express* **10** (2007) 6010.
[105] C. Torres-Torres, A.V. Khomenko, J.C. Cheang-Wong, L. Rodriguez-Fernandez, A. Crespo-Soso and A. Oliver // *Opt. Express* **15** (2007) 9248.
[106] B. Ghosh, P. Chakraborty, B. Sundaravel and C. Vijayan // *Nucl. Instr. Meth. Phys. Res. B* **266** (2008) 1356.
[107] Y.H. Wang, J.D. Lu, R.W. Wang, S.J. Peng, Y.I. Mao and Y.G. Cheng // *Physica B* **403** (2008) 3399.
[108] Y.H. Wang, J.D. Lu, R.W. Wang, Y.I. Mao and Y.G. Cheng // *Vacuum* **82** (2008) 1220.
[109] G. Battaglin, P. Calvelli, E. Cattaruzza, P. Polloni, E. Borsella, T. Cesa and P. Mazzoldi // *J. Opt. Soc. Am. B* **17** (2000) 213.
[110] R.H. Magruder III, D.H. Osbone and R.A. Zuhr // *J. Non.-Cryst. Solids* **176** (1994) 299.
[111] Y.H. Wang, C.Z. Jiang, F. Ren, Q.Q. Wang, D.J. Chen and D.J. Fu // *J. Mat. Sci.* **42** (2007) 7294.
[112] Y.H. Wang, C.Z. Jiang, X.H. Xiao and Y.G. Cheng // *Physica B* **403** (2008) 2143.
[113] Y.H. Wang, Y.M. Wang, C.J. Han, J.D. Lu, L.L. Ji and R.W. Wang // *Physica B* **405** (2010) 2848.
[114] Y.H. Wang, Y.M. Wang, C.J. Han, J.D. Lu, L.L. Ji and R.W. Wang // *Vacuum* **85** (2010) 207.
[115] E. Cattaruzza, G. Battaglin, F. Gonella, P. Calvelli, G. Mattei, C. Maurizio, P. Mazzoldi, S. Padovani, R. Polloni, C. Sada, B.F. Scremin and F.D'Acapito // *Composites Sci. Technol*. **68** (2003) 1203.
[116] E. Cattaruzza, G. Battaglin, F. Gonella, P. Calvelli, G. Mattei, C. Maurizio, P. Mazzoldi, R. Polloni and B.F. Scremin // *Appl. Surf. Sci.* **247** (2005) 390.
[117] R.H. Magruder III, R.A. Zuhr and D.H. Osbone // *Nucl. Instr. Meth. Phys. Res. B* **99** (1995) 590.
[118] G. Mie // *Ann. Phys*. **25** (1908) 377.
[119] B. Palpant, In: *Non-Linear optical properties of matter*, ed. by by M.G. Papadopoulos (Springer: Amsterdam, 2006).
[120] M. Sheik-Bahae, AA. Said and E.W. van Stryland // *Opt. Lett*. **14** (1989) 955.
[121] M. Sheik-Bahae, AA. Said, D.J. Hagan and E.W. van Stryland // *IEEE J. Quan. Elect.* **26** (1990) 760.
[122] C.H. Kwak, Y.L. Lee and S.G. Kim // *J. Opt. Soc. Am*. **16** (1999) 600.
[123] A.L. Stepanov, V.A. Zhikharev, D.E. Hole, P.D. Townsend and I.B. Khaibullin // *Nucl. Instr. Meth. Phys. Res. B* **166-167** (2000) 26.
[124] J.F. Reintjes, *Nonlinear-optical parametrical processes in liquids and gases* (Academic: Orlando, 1984).
[125] S.V. Karpov, A.K. Popov and V.V. Slabko // *JETP Lett.* **66** (1997) 106.
[126] R.A. Ganeev, A.I. Ryasnyansky, S.R. Kamalov, M.K. Kodirov and T. Usmanov // *J. Phys. D: Appl. Phys.* **34** (2001) 56.

[127] L.W. Tutt and T.F. Boggess // *Prog. Quant. Electr.* **17** (1993) 299.
[128] Y.R. Shen, *The principles of nonlinear optics* (Wiley: New York, 1989).
[129] A. Owyoung // *IEEE J. Quant. Electr*. **9** (1973) 1064.
[130] S.C. Mehendale, S.R. Mishra, K.S. Bindra, M. Laghate, T.S. Dhami, K.C. Rustagi // *Opt. Comm*. **133** (1997) 273.
[131] M. Falconieri // *J. Opt. A: Pure Appl. Opt.* **1** (1999) 662.
[132] G. Battaglin, P. Calvelli, E. Cattaruzza, F. Gonella, R. Polloni, G. Mattei and P. Mazzoldi // *Appl. Phys. Lett.* **78** (2001) 3953.
[133] V. Mizrahi, K.W. DeLong, G.I. Stegeman, M.A. Saifi and M.J. Andejco // *Opt. Lett.* **14** (1989) 1140.
[134] R. Rangel-Rojo, T. Kosa, E. Hajto, P.J.S. Ewen, A.E. Owen, A.K. Kar and B.S. Wherrett // *Opt. Comm*. **109** (1994) 145.
[135] S.R. Fribers and P.W. Smith // *IEEE J. Quant. Electr*. **23** (1987) 2089.
[136] M.J. Moran, C.Y. She and R.L. Carman // *IEEE J. Quant. Electr*. **11** (1975) 259.
[137] T. Xia, D.J. Hagan, M. Sheik-Behae and E.W. van Stryland // *Opt. Lett*. **19** (1994) 317.
[138] H. Ma, A.S.L. Gomes and C.B. de Araujo // *Appl. Phys. Lett.* **59** (1991) 2666.
[139] D.V. Petrov, A.S.L. Gomes and C.B. de Araujo // *Appl. Phys. Lett.* **65** (1994) 1067.
[140] D.V. Petrov, A.S.L. Gomes and C.B. de Araujo // *Opt. Comm*. **123** (1996) 637.
[141] D.V. Petrov // *J. Opt. Soc. Am*. **13** (1996) 1491.
[142] T. Kawazoe, H. Kawaguchi, J. Inoue, O. Haba and M. Ueda // *Opt. Comm*. **160** (1999) 125.
[143] A.L. Stepanov // *Rev. Adv. Mater. Sci*. **4** (2003) 45.
[144] M. Martinelli, L. Gomes, R.J. Horowicz // *Appl. Opt.* **39** (2000) 6193.
[145] R.A. Ganeev and A.I. Ryasniansy // *Phys. Stat. Sol.* A **202** (2005) 120.
[146] A.L. Stepanov and V.N. Popok // *Surf. Sci.* **566-568** (2004) 1250.
[147] A.L. Stepanov, U. Kreibig, D.E. Hole, R.I. Khaibullin, I.B. Khaibullin and V.N. Popok // *Nucl. Instr. Meth. Phys. Res. B* **178** (2001) 120.
[148] S.V. Karpov, F.K. Popov and V.V. Slabko // *Izv. Akad. Nauk SSSR Ser. Fiz*. **60** (1996) 42.